FAMU-FSU College of Engineering
Department of Electrical and Computer Engineering

SYSTEM-LEVEL DESIGN REVIEW

EEL4911C – ECE Senior Design Project I

Project Title: **Synthetic Active Array Radar Aperture (SAR)**

Team #: E11

Student Team Members:

- **Matthew Cammuse**, Electrical Engineering (Email: mgc11@my.fsu.edu)
- **Joshua Cushion**, Electrical Engineering (Email: jlc10e@my.fsu.edu)
- **Patrick Delallana**, Electrical/Computer Engineering (Email: pnd10@my.fsu.edu)
- **Julia Kim**, Electrical Engineering (Email: jk09k@my.fsu.edu)
- **Malcolm Harmon**, Mechanical Engineering (Email: mjh11f@my.fsu.edu)
- **Benjamin Mock**, Industrial Engineering (Email: bam11g@my.fsu.edu)
- **Mark Poindexter**, Mechanical Engineering (Email: mpp12b@my.fsu.edu)
- **Jasmine Vanderhorst**, Industrial Engineering (Email:Vanderhorst_91@yahoo.com)

Senior Design Project Instructor: Dr. Michael Frank
Electrical/Computer Engineering Department Advisors: Dr. Simon Foo and Dr. Shonda Bernadin
Industrial Engineering Department Advisor: Dr. Okoli
Mechanical Engineering Department Advisor: Dr. Collins

Submitted in partial fulfillment of the requirements for
EEL4911C – ECE Senior Design Project I

November 13, 2014

Project Executive Summary

The purpose of the electronic Synthetic Active Aperture Radar (SAR) Imager project, sponsored by Northrop Grumman, is to design and develop a low-cost detection system capable of providing a low, but useful, imagery resolution as a learning experience. In theory, the application of the electronic SAR Imager focuses on security applications and its ability to detect potentially threatening objects such as handguns. This project is sponsored through the FAMU-Foundation with a $50,000.00 budget with an expected timeline of eight months to completion.
A radar is an object detection system that uses radio waves to measure characteristics of certain objects and is typically composed of antennas in which transmit pulses of radio waves bounce off the target in the designated range. The wave is reflected off the target and returns a wave to the receiving end of the system which is usually a dish, horn, or some form of waveguide usually located at the same site as the transmission of the wave. In a typical radar, the antenna which usually acts as a transmitter and/or receiver is in a static position. An SAR is a form of radar imaging. This can be seen such applications as aircraft topography; the antenna on the plane would transmit signal to a landscape while the antenna is moving. To create a fixed electronic SAR imager, the design will be constructed with multiple stationary antennas that emit or receive pulses to emulate the theory of an SAR.

This project will consist of twenty horn antennas: sixteen receive and four transmit. The antenna structure will consist of two linear antenna apertures. Each aperture will contain eight receive antennas placed between two transmit antennas. Two antenna apertures will be utilized and laid across each other creating a T-shaped design with each horn directed towards the target. Besides the center horn antennas, each horn will be angled directionally towards the target. Overall, the design will create four rows of five antennas being placed at a 90º to each other, creating sixteen phase centers per linear antenna aperture and thirty-two phase centers for the whole design. A phase center is the half-way distance between one transmit and one receive antenna in an aperture and represents a receive antenna's center absorbance point or maximum absorbance point. One transmit is responsible for eight phase centers. When placing receive antennas next to each other, additional maximum absorbance points are created. One aperture may only have eight receive antennas but eight additional phase or maximum absorbance points are created. More phase centers results in a better chance to receiving a return signal. For this project, radar system is required to reach a target twenty feet away and cover a human's body.

The system will be controlled via an FPGA which will sequentially transmit pulse from an antenna and then turn on the receiving antennas/turn off the transmitting antenna pulse to receiving a signal bouncing off the target. This will be done from every 90º direction one after the other to give the most data possible. The data would get sampled on a scope and get recorded. If time permits, the FPGA can do more complicated tasks such as storing some of the data that can be output and operated on. This sampled data could then be captured and sent to a PC for image processing. This would most likely be done using software such as Simulink. Overall the goal of this project is to apply engineering design practices and technical knowledge to create a limited prototype of an SAR Imager which would transmit and receive pulse from at least one row of antennas out of the four 90º rows.

Contents

1 Introduction

1.1 Acknowledgements

The electronic Synthetic Active Aperture Radar (SAR) Imager team would like to extend thanks to the stakeholders of this project from Northrop Grumman and the FAMU-FSU College of Engineering sponsors. First and foremost to the corporate sponsors at Northrop Grumman, we are most grateful for the generous $50,000 financial contribution to the FAMU Foundation to support research, equipment procurement, and work efforts on the project. In addition to financial contributions, the team also thanks Northrop Grumman for resource support from Peter Stenger, who continually provided technical support, guidance, and direction throughout the duration of the project. We would like to thank Dr. Michael Frank, Dr. Simon Foo, Dr. Shonda Bernadin, Dr. Bruce Harvey, and Dr. Rajendra Arora from the Electrical & Computer Engineering Department for their continued efforts to advise the team in making practical engineering design decisions. Also, we would like to thank Dr. Nikhil Gupta, Dr. Scott Helzer, Dr. Emmanuel Collins, Ricardo Aleman, and Samuel Botero from the Mechanical Engineering department for their contributions in developing professionalism, providing continuous feedback for improvement, and supporting the mechanical design of the SAR Imager system. Finally, we thank Dr. Okenwa Okoli, Dr. James Dobbs, Emily Hammel, and Margaret Scheiner from the Industrial Engineering department for their help in project management, scheduling, and quality engineering.

1.2 Problem Statement

1.2.1 General Problem Statement

The number one priority of this project is to create a limited prototype of a radar system with synthetic-aperture radar theory using COTS (commercial off the shelf) components. The theory behind an SAR Imager requires a one moving antenna that acts as a transmitter and a receiver. As the antenna is in motion it transmits signals and receives the reflected radiation scatterings from the target, this allows it to generate an image of an entire area. Since a moving antenna is outside of the scope of the class, the design will supplement the framework of a single moveable antenna with a system having multiple antennas to emit and receive signal from different locations. The theory behind transmitting and receiving signals on a single target from multiple locations will still be implemented, however the design will contain multiple antennas.

1.2.2 General Problem Solution

The solution will be tackled in several steps. There are three disciplines to this project: Electrical/Computer Engineering, Mechanical Engineering, and Industrial Engineering.

The Electrical/Computer Engineers will design a stationary prototype of a radar system which has twenty antennas overall with sixteen being receive antennas and four being transmit antennas. These antennas will be separated into four rows of five antennas each. Each of these four rows will be placed 90º to each other, and there will be an epicenter between these four rows

which is where the target will be. The system that controls the transmission and receiving of signal from the antennas will be controlled via an FPGA. It is the job of the Electrical/Computer engineers to design a workable prototype of the system that will transmit and receive signals from antennas. This also includes the programming of the FPGA board, signal processing, and possibly even image processing of data if the project goes further than expected. The Electrical/Computer Engineers will be the ones to determine almost all of the theory and components of the system, thus making them the base of the project.

The Mechanical Engineers will design the physical structure of the antennas and the associated horns that go with them. The Mechanical engineers will work very closely with the Electrical engineer who specializes in antennas to design the proper horn shape and the spacing between each of the antennas. The Mechanical Engineers also have a role in helping the Electrical Engineers set up all of the components and equipment of the system and making sure that they are working properly as well. It is vitally important for the Mechanical and Electrical Engineers to work in close contact since the Mechanical portion of this project deals with the physical design of the antennas which transmit and emit signal.

The Industrial Engineers have a primary role in managing the human factors, risk analysis, the project schedule, and the overall budget of the system. The Industrial Engineers will also be in charge of helping the Electrical Engineers acquire and order the specific components needed for the system. Industrial Engineers will also be in close contact with the school and the sponsor since they will be the ones who actually go and submit the orders for purchase. Industrial Engineers will also be of utmost importance when making administrative decisions within the team due to their knowledge of cost engineering and optimization.

1.3 Operating Environment

The operating environment will be those locations of primary concern for homeland security applications such as airports, public schools, museums, etc. These locations will demand that the SAR Imager properly functions at average room temperature (293.15 – 298.15 K) and within average humidity (30 – 50%) [1]. The SAR Imager should be able to operate in the presence of other electronics and RADARs and not be influenced by them in their main operation: determining the hidden threat of hidden weaponry. This system should be able to operate at a nonstop pace when needed and also be equipped with adjustments to be set-up in the specified location on interest.

1.4 Intended Use(s) and Intended User(s)

1.4.1 Intended Use

The intended use for the SAR Imager will be for theoretical implementation and testing. Tests to check for the transmission and receiving of pulse by the antennas of this project will be the primary use for the system. A mannequin will act as the target to abide by FSU campus medical standards. If time allows, more complicated aspects such as image processing can be used to generate an image.

1.4.2 Intended Users

The intended users for the SAR Imager will be the student members of the team. Any advisors or the sponsor may want to test out the system for themselves to check progress and that is a viable option as well. As a research project, this project only intends to be used as a prototype. The end result should have a physical system that transmits and receives reflected radiation scatterings from a target.

1.5 Assumptions and Limitations

1.5.1 Assumptions

This project is based upon the following assumptions:

- The radar should operate at frequencies safe for human interaction.
- The radar must be capable of detecting metal and/or threatening objects on a person's body from a distance.
- The radar must be operating at near real-time.
- The data from the receiver should generate polynomial images on a display screen. Then based on color identification, it should be easy to pin point an object's location. A selected color would represent a received signal, and if that color appears on the screen, an object has been located. .
- The FPGA board should have Peripheral Module (Pmod) connectors to add analog-to-digital (A/D) converters.

1.5.2 Limitations

The decisions in this project are confined by the following limitations:

- The distance to the scene to be imaged must be 20 feet. (REQF-002)
- The area to be imaged, also known as scene extent, must cover the width of a person and should ideally cover the person's torso and legs. However, the scene extent will be based on the type of horn antennas selected. (REQF-003)
- The frequency range should be within the X- or Ku- band operating frequency, which is a range of 8 to 12 GHz for X-band and 12 to 18 GHz for Ku-band. (REQF-001)
- The cross range and down range resolution are determined based on the employed beamwidth and distance between the antennas and target. (REQF-004)
- The down range resolution must be low so it does not take a thorough image of the body, but has enough depth. (REQF-005)
- The pulse width should be at about 20 nanoseconds so the pulse can travel to and from the scene. (REQF-006)
- The number of phase centers for the system is sixteen. (REQF-010)
- The number of antennas to be used for the system is sixteen receive antennas and four transmit antennas. (CONS-001)

- Antennas must be placed close together at equal distances apart and be precisely pointed at target. (CONS-002)
- To use the system for testing, the room must be bigger than 20 feet x 15 feet.

1.6 Expected End Products and Other Deliverables

1.6.1 Synthetic Active Aperture Radar Imager

The SAR Imager system will be designed and physically implemented by April 2015. The sponsor in particular does not have a deadline, but the College of Engineering's deadline for completion of projects is April 2015. The end product of this project will be a testable conceptual design of an electronic SAR Imager. The electronic SAR Imager will have the ability to receive and transmit pulses on at least one row of antennas out of the four 90º rows on the whole prototype. A summary of the radar system's components are listed below:

- 1 Field Programmable Gate Array (FPGA) board
- 4 Transmit Antennas
- 16 Receive Antennas
- 1 Voltage Controlled Oscillator (VCO)
- 1 IQ Demodulator
- 1Single Pole Double Throw (SPDT) Switch
- 1Single Pole Four Throw (SP4T) Switch
- 1Single Pole Sixteen Throw (SP16T) Switch
- 2 Frequency Multipliers
- 2 Low Noise Amplifiers (LNA)
- 1 Wideband Amplifier
- 3 Fixed Attenuators
- 2 Variable Attenuators
- 1 Power Amplifier
- 1 Isolator
- 2 Band Pass Filters (BPF)
- 1 Level Shift Circuit
- 1 VGA Display
- 2 Analog-to-Digital Converters
- 1 Power Supply Board
- 1 Computer

1.6.2 Documentation and Configuration Flash Drive

1.6.2.1 Electronic Circuit Schematics

The electronic circuit model developed will be saved in different formats to the Documentation and Configuration flash drive. This will be completed by April 2015.

1.6.2.2 Antenna Structural Schematics

The structural design of the antennas and the supporting system will be be saved to the Documentation and Configuration flash drive. This will be completed by April 2015.

1.6.2.3 Code and Configuration Files

The VHDL code and configuration files developed for the electronic SAR imager will be organized in a .zip file and saved into the Documentation and Configuration flash drive. This will be completed by April 2015.

2 Overall System and Subsystem Design

2.1 Overview

2.1.1 Electrical System Overview

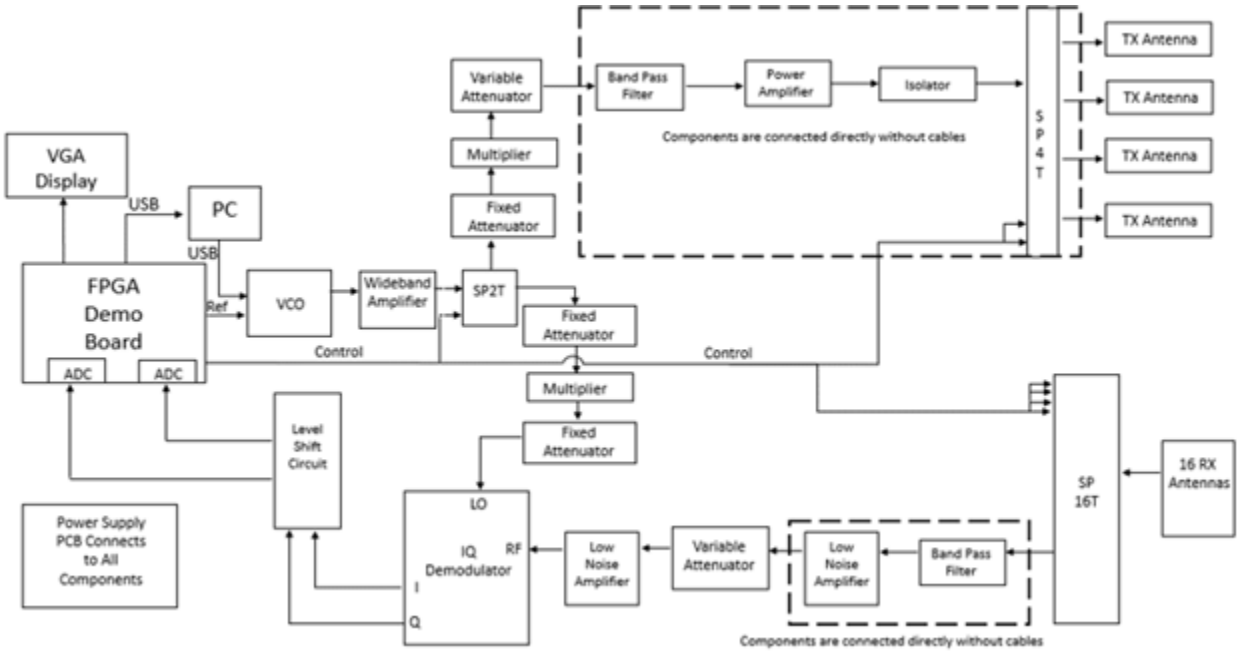

Figure 1. Block Diagram of the Electrical System

The diagram in Figure 1 shows the electrical system of the multiple antenna radar system. The electrical system is responsible for generating the radio frequency signal that transmits into the scene extent; this is accomplished using a voltage controlled oscillator along with a power amplifier to amplify the power and the 4 transmit antennas to emit the signal. The electrical subsystem is also responsible for receiving the reflected waveform scatterings of the return signal from the target and converting them to digital voltages in order to do the signal processing. This is accomplished through the use the 16 receive antennas, the IQ demodulator,

the analog to digital converters, the FPGA and the other components in the receive chain. Another responsibility of this subsystem is to perform the signal processing to generate the imagery. This will be conducted by the computer using signal processing software. Lastly the electrical subsystem will display the imagery on the VGA display.

2.1.2 Antenna Design Overview

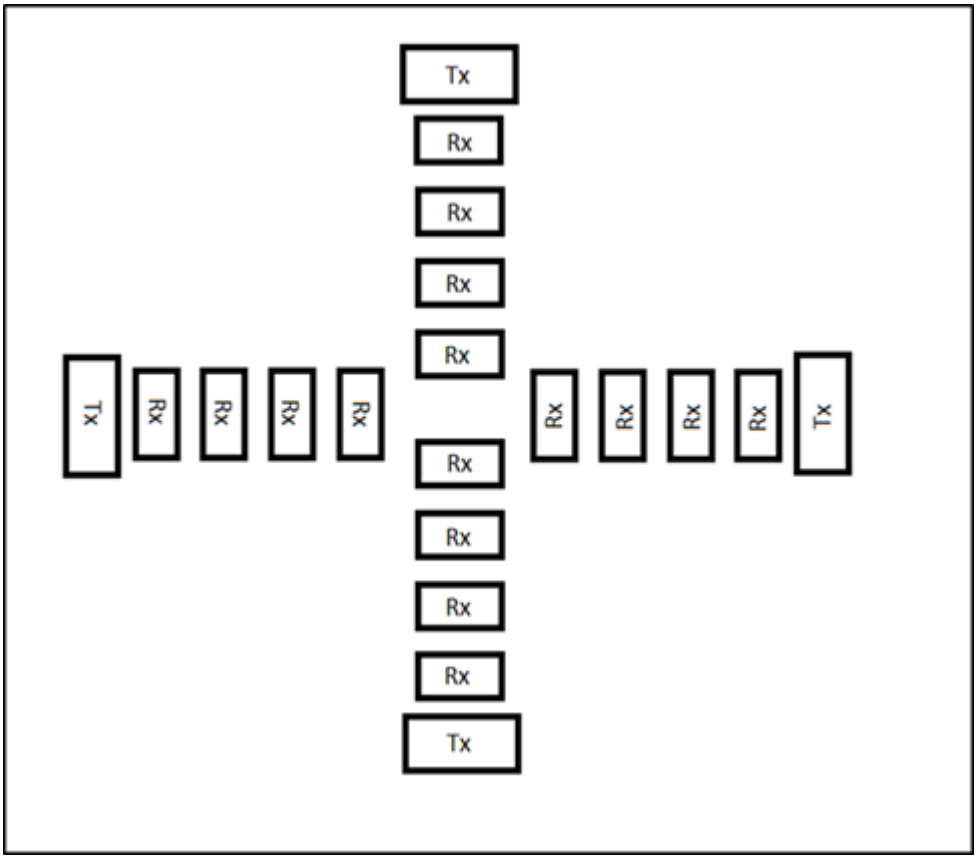

Figure 2. T-Shaped Linear Array Antenna Design

The antenna design will consist of two linear antenna arrays. Each array will have two transmit antennas located at the ends of each array with eight receive antennas between the transmit antennas. The two arrays will then cross each to form a T-shaped design illustrated in Figure 2. X-band, 17 dB gain, rectangular horn antennas will be utilized for the design. Spacing between transmit and receive antennas will be three lambda (3λ), and spacing between receive transmit antennas is six lambda (6λ). The spacing distances will prevent grating lobes from entering into the scene extent as the main lobe scans the scene. When the antenna is transmitting, the design will allow the beam to cover an area of nine feet by nine feet, which is more than the 30 by 30 inch scene extent. Each antenna will connect to an iso-adapter – iso-apapter changes a signal between coaxial to waveguide. Coaxial cables will connect to each iso-adapter and communicate to the rest of the radar system.

2.1.3 Antenna Structure Overview

The objective of this structure is to hold the antennas in the correct position. This is essential because each horn must send out a pulse that will hit the appropriate target and also receive those pulses. The height of the structure is also equally important, because this will make the transmission of pulses easier if it can be fixed to a horizontal plane aligned with the target. The structure is made of four quadrants that will be attached at each end by a c bracket. Wires will connect to the back of the antenna horns and travel along the back plate in a hidden position and connect to the proper components in the component box. The details of this can be seen in further description below.

2.1.4 Signal Processing Overview

In order to form an image on the display, it is necessary to process the signal that is being received and use that to determine where energy is coming in from and at what angles. Basis functions would be determined for each of the sixteen phase centers at certain angles and stored in the memory of the FPGA board. The IQ demodulator used in the electrical system will provide the data to be used for signal processing, and the fast Fourier transform calculations would be done in the computer. The calculations realized will generate the peaks that determine where the scatters are, and this information can be coordinated with the display to light up the correct pixels at a certain area in order to form the image.

2.2 Electrical System

2.2.1 Transmit Signal Chain

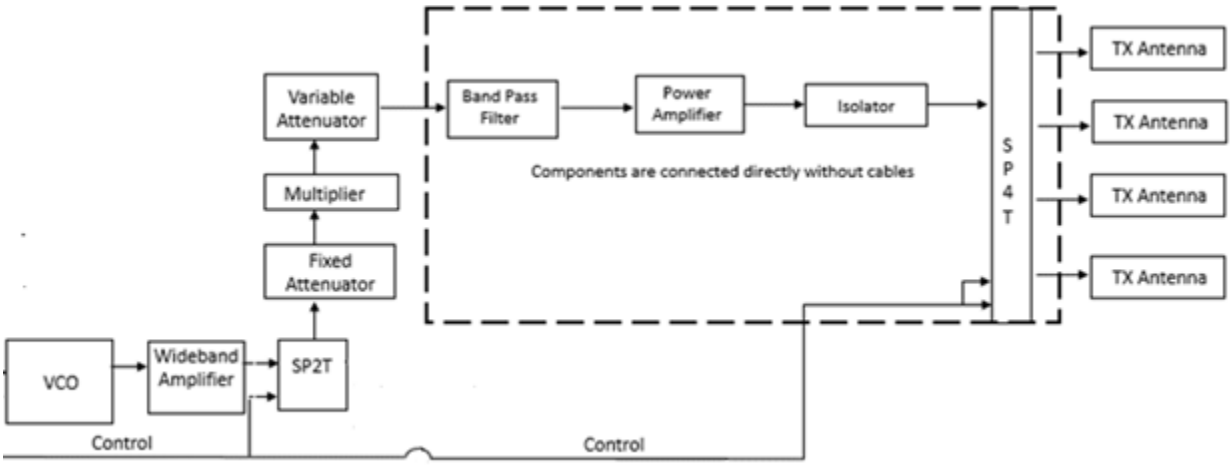

Figure 3. Transmit Signal Chain

The purpose of this subsystem is to generate and transmit a radio frequency (RF) signal that will be emitted into the area to be scanned by the radar. This subsystem is also responsible for establishing a operating frequency for the entire radar. The signal generation starts with the voltage controlled oscillator (VCO). The VCO used in the design has an output power of -4dBm (0.398 mW) and operates at a frequency range of 4.38 GHz – 5.1 GHz. The next component in the signal transmit chain is the wideband amplifier. This amplifier was placed here because it was needed to provide enough input power into the X2 multiplier. The gain of this amplifier is 26dB. An important concept that was taken into consideration is the 1dB compression point (P1dB). This is the point in which the gain for linear amplifiers is no longer fixed for that specific frequency range. It is at this point where the output power becomes compressed and is no longer linearly proportionate to the input power. The P1dB for this component is 24 dBm, thus while completing the analysis the output power from the wideband amplifier was confined to less than 24 dBm. Also it is good engineering practice to leave a margin of error when calculating the output power therefore the output power from this component was designed to be 21 dBm (125.9 mW). The VCO and wideband amplifier are connected by a cable of which the assumed gain is -1 dB (0.794 magnitude of loss). The next component in the chain is single pole double throw (SPDT) switch. This component allows the radar to switch between transmit and receive modes. The SPDT switch has a P1dB value of 27 dBm and a gain of -2 dB; with an input power of 20 dBm the output power from the SPDT was calculated to be 18 dBm. The next major component in the signal transmit chain was the X2 frequency multiplier. The purpose of the frequency multiplier is to double the input frequency. As stated before, the frequency generated by the VCO is in the range of 4.38 GHz – 5.1 GHz, once the signal reaches the frequency multiplier it is then doubled to the desired range of approximately 10 GHz. The frequency multiplier has a required input power of 6 dBm and an absolute maximum input power level of 13 dBm. Once this input power level is reached, the frequency multiplier then behaves like a power source because it will generate 14 dBm of power. Due to the restriction of the input power to the frequency multiplier being 13 dBm, a fixed attenuator was added to the signal transmit chain between the SPDT and the frequency multiplier. The attenuation level set in the calculations is -10 dB; this is considered a loss to the overall gain of the chain. The purpose of using a fixed attenuator here instead of a variable attenuator is that the attenuation does will not need to be adjusted at this point in the chain.

The next component in the transmit signal chain is a variable attenuator. This variable has a P1dB compression point of 37 dBm and the attenuation was set to -10dBm. The input power into this component was 13 dBm results in an output power of 3 dBm. This attenuator precedes a band pass filter as well as power amplifier. The main consideration that was kept in mind was the power amplifier. The power amplifier has a gain of 32 dB and a P1db compression value of 30 dBm. This meant that the output power from the amplifier had to be less than 30 dBm which it was calculated to be 29 dBm. The band pass filter was used to provide a more accurate frequency for the transmit signal chain. Its center frequency value is 10.5 GHz which is aligned with the frequency that the customer specified. The band pass filter contributes a gain of -3dB to the chain. The next component in the chain is the isolator. The purpose of the isolator is to restrict

power from flowing in the reverse direction. The isolator has a gain of -1.5 dB and must not receive more input power than 29 dBm. The value of input power calculated into the isolator was 29 dBm which resulted in an output power of 27.5 dBm. After the single pole four throw (SP4T) switch follows the isolator. The SP4T is used to switch the output signal from being emitted by the four transmit antennas. It has a P1db compression point of 37 dBm and a gain of -2 dB. The output power calculated from this component was 25.5 dBm and was followed by a cable gain of -1 dB. The final transmit power generated by this chain was 24.5 dBm. The overall goal in the analysis of the transmission chain is to calculate the power progressed through the path up until the antennas. This is the value that was used in the signal to noise ratio equation. This was accomplished by accounting for the gains and losses of the components in the chain. The transmit power of this signal is to be within the limits of safety as set by the rules regarding safe human exposure to electromagnetic RF fields, set forth by the Federal Communications Commission (FCC). The limit is 10 W/m^2, at the distance of 6 meters our peak transmit power of 24.5 dBm (282 mW) is well within the safety limits.

Components	Input Power (dBm)	Gain (dB)	Output Power (dBm)	P1db Compression (dBm)
VCO	0	0	-4	n/a
Cable	-4	-1	-5	n/a
Wideband Amplifier	-5	26	21	24
Cable	21	-1	20	n/a
SPDT	20	-2	18	27
Cable	18	-1	17	n/a
Fixed Attenuator	17	-10	7	n/a
Cable	7	-1	6	n/a
X2 Frequency Multiplier	6	0	14	n/a
Cable	14	-1	13	n/a
Variable Attenuator	13	-11	2	37
Cable	2	-1	1	n/a
Band Pass Filter	1	-3	-2	n/a
Cable	-2	-1	-3	n/a
Power Amplifier	-3	32	29	30
Isolator	29	-1.5	27.5	n/a
SP4T	27.5	-2	25.5	37
Cable	25.5	-1	24.5	n/a

Table 1: Transmit Signal Chain Power Calculations

2.2.2 Receive Signal Chain

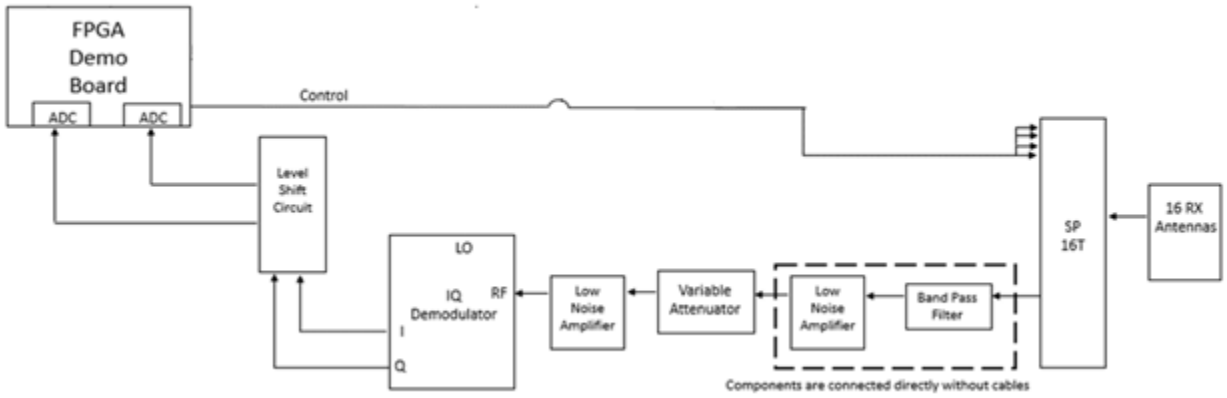

Figure 4. Receive Signal Chain

The purpose of this subsystem is to receive the RF signal scatterings that are reflected from the target and convert those signals to digital voltages to be used in the signal processing. The analysis for this chain includes calculating the power of the signal that it transmitted through this chain as well as the noise figure and noise temperature contributed by each component. The noise figure for components that have a negative gain (loss) is equal to that gain in dB. For components with a positive gain the noise figure is given in the datasheet. The equation for noise temperature for all components is shown below:

$$\boldsymbol{nt = 290°K(10^{\frac{nt(dB)}{10}} - 1)}$$

Equation 1: Noise Temperature

The actual signal power received by the receive antenna is discussed in a later section; for now this value is to be considered as -46.3 dBm. This value seen by the input to the single pole 16 throw (SP16T) switch is added to the gain of -1 dB from the cable. In total the calculated input power to the SP16T was -47.3 dBm. The SP16T switch has a gain of -4.7 dB and a P1db compression point of 24 dBm. The calculated output power of the SP16T switch is -52 dBm which is well below the 24 dBm compression value. Also because the SP16T switch has negative gain the noise figure is equal to 4.7 dB. The next component in the receive signal chain is the band pass filter. The band pass filter is used to provide precision to the frequency of the received signal scatterings reflected off of the target. The calculated received power for this component is -53 dBm, the gain is -3 dB and the output power is -53 dBm. The next component in this chain is a low noise amplifier. This component is used to amplify the power of the receive signal and amplify the noise as least as possible. The gain of this amplifier is 38 dB which results in a calculated output power of -19 dBm. The calculated output power of this component is less than the P1dB compression point which is 24 dBm. The noise figure listed in the data sheet is 2.2 dB. A variable attenuator was placed in the chain after the low noise amplifier. The purpose of using

a variable attenuator is to allow for the power in the chain after this point to be adjusted. In the calculations the attenuation used was -4 dB. This will limit the input power to the RF channel of the IQ demodulator. The next component in the chain is another low noise amplifier. This was added to increase the signal power input into the RF channel of the IQ demodulator. In short the reason that the input power of the RF channel of the IQ demodulator deals with the output DC voltage that will be generated by the IQ demodulator. This concept will be elaborated on later in the paper. The point to note now is that the output power of this low noise amplifier was calculated as 13 dBm due to the gain of 38 dB.

	Cable	SP16T	Cable	band pass filter	Cable	Low Noise Amplifier	CONTINUE
Pin (dBM)	-46.295	-47.295	-51.995	-52.995	-55.995	-56.995	
Gain (dB)	-1	-4.7	-1	-3	-1	38	
Gain (magntude)	0.794	0.339	0.794	0.501	0.794	6309.573	
Pout (dBM)	-47.295	-51.995	-52.995	-55.995	-56.995	-18.995	
Pout (mW)	1.86E-05	6.32E-06	5.02E-06	2.51E-06	2.00E-06	0.012604	
Pout (W)	1.86E-08	6.32E-09	5.02E-09	2.51E-09	2.00E-09	1.26E-05	
NF (dB)	1	4.7	1	3	1	2.2	
NF	1.259	2.951	1.259	1.995	1.259	1.660	
NF (cascade)	1.259	3.715	4.677	9.333	11.749	19.498	
Noise Temp (K)	75.08837	565.8507	75.08837	288.6261	75.08837	191.2802	
Noise Temp cascade (K)	97.5168	392.2338	561.399	2196.866	4048.06	25547.03	

Table 2: Receive Chain Calculations (part1)

	CONTINUE	Cable	Variable Attenuator	Low Noise Amplifier	Cable	RF (IQ Demodulator)
Pin (dBM)		-18.995	-19.995	-24.995	13.005	12.005
Gain (dB)		-1	-5	38	-1	-7
Gain (magntude)		0.794	0.316	6309.573	0.794	0.200
Pout (dBM)		-19.995	-24.995	13.005	12.005	5.005
Pout (mW)		0.010012	0.003166	19.9764	15.86782	3.166046
Pout (W)		1.00E-05	3.17E-06	0.019976	0.015868	0.003166
NF (dB)		1	5	2.2	1	7
NF		1.259	3.162	1.660	1.259	5.012
NF (cascade)		19.499	19.504	19.505	19.506	19.536
Noise Temp (K)		75.08837	627.0605	191.2802	75.08837	1163.443
Noise Temp cascade (K)		25549.9	25580.08	25586.3	25591.51	25769.36

Table 3: Receive Chain Calculations (part 2)

2.2.3 IQ Demodulator

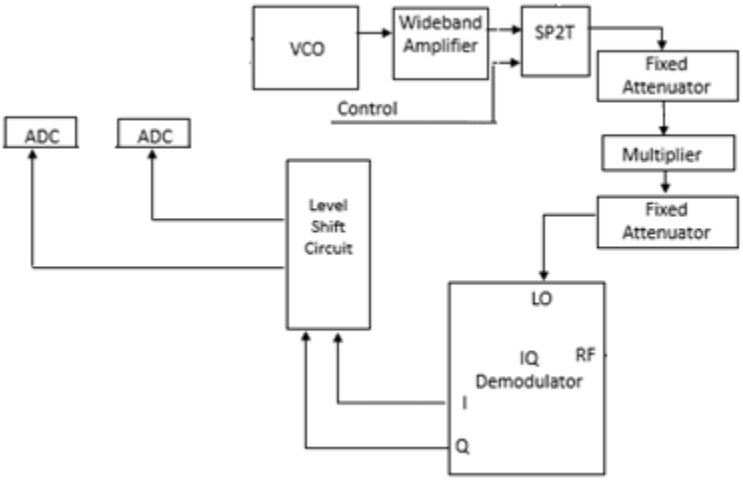

Figure 5. IQ Demodulator Chain

The IQ demodulator is a key component in the electrical system. It is used to relay the amplitude and phase of the incoming RF signal to the analog to digital converters. The IQ Demodulator converts the amplitude and phase information to DC voltages. This is done based on the theory of the IQ demodulator. In short this process involves generating a amplitude from the I(t) and Q(t) signals. The amplitude is generated using the equations shown below:

$$A(t) = \sqrt{I^2(t) + Q^2(t)}$$

Equation 2: Amplitude of RF signal input to IQ Demodulator

$$\phi(t) = \arctan\left(\frac{Q(t)}{I(t)}\right)$$

Equation 3: Phase of RF signal input to IQ Demodulator

The input power to the RF channel of the IQ demodulator was calculated to be 12 dBm, the IQ demodulator has a conversion loss of 7 dB, resulting in an output power of 5 dBm (3.16 mW). The output impedance of this component is 50Ω. The next step in the analysis was to calculate the voltage range of the I and Q outputs. This was done by using the equation below:

$$V_{dc} = \sqrt{Pout(W) + Zout(\Omega)}\ (V)$$

Equation 4: Output voltage range

This led to a calculated value for the maximum voltage output by the IQ demodulator as 397.8 mV, which occurs when the phase angle is 45° between signals I(t) and Q(t). However

when the phase angle between the two signals is -45° the output voltage of the IQ demodulator is -397.4 mV, which results in an output voltage range of approximately -400 mV to 400 mV. The DC offset error of this particular model IQ demodulator is +/-4mV. As state before the large increase in gain in the receive path due to the two low noise amplifiers is necessary to increase the power of the input signal in order to allow the IQ demodulator to produce a DC voltage that is high. The DC output voltage needs to be high in order to make the DC offset error negligible. At 4 mV to 400 mV the DC offset error 10% of the output voltage. This is causes the DC offset to be negligible which is desirable.

This process occurs when a signal is input into the LO channel of the IQ demodulator or in other words when the SPDT switch is not driving the transmit signal chain. This is the reason for the SPDT switch which switches the radar between transmit and receive modes. The input signal must have a power of 5 dBm. This is the reason for the variable attenuator that comes after the SPDT switch, it is necessary to decrease the signal power that is amplified by the wideband amplifier to 5 dBm.

Components	Input Power (dBm)	Gain (dB)	Output Power (dBm)	P1db Compression (dBm)
VCO	0	0	-4	n/a
Cable	-4	-1	-5	n/a
Wideband Amplifier	-5	26	21	24
Cable	21	-1	20	n/a
SPDT	20	-2	18	27
Cable	18	-1	17	n/a
Fixed Attenuator	17	-10	7	n/a
Cable	7	-1	6	n/a
X2 Frequency Multiplier	6	0	14	n/a
Cable	14	-1	13	n/a
Fixed Attenuator	13	-7	6	37
Cable	6	-1	5	n/a
LO IQ Demodulator	5	n/a	n/a	n/a

Table 4. LO IQ Demodulator Signal Chain Power Calculations

2.2.4 Level Shift Circuit

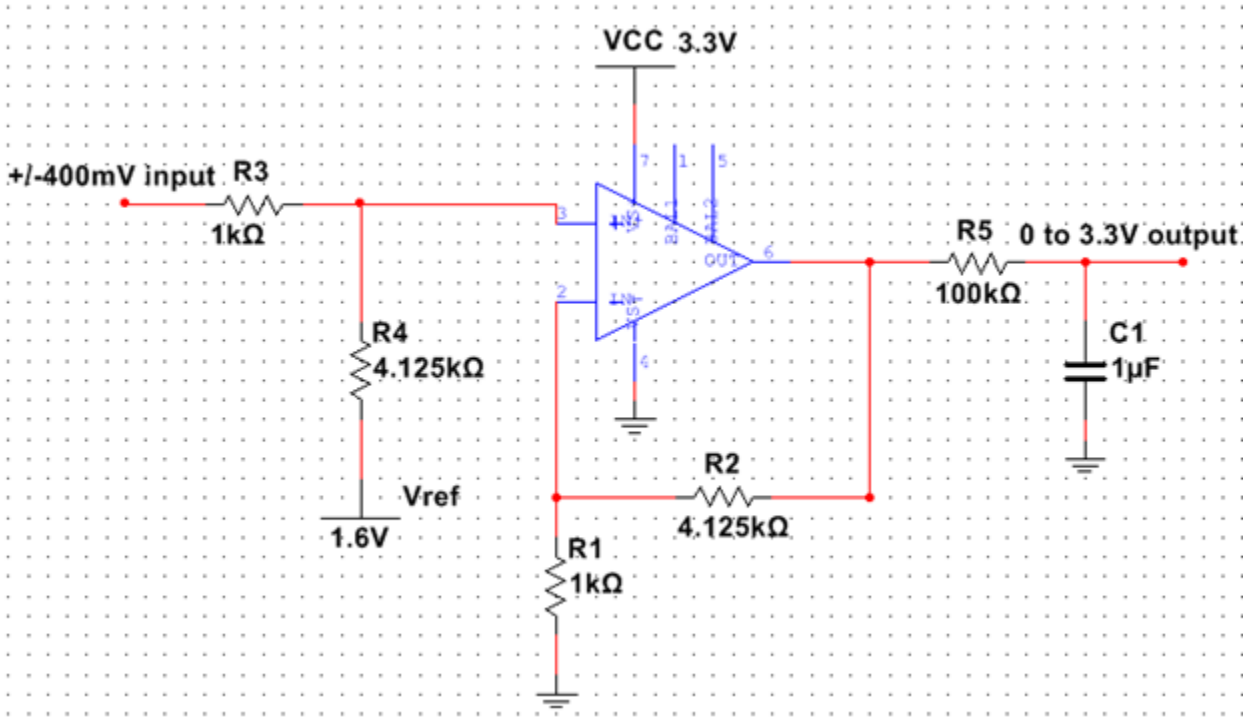

Figure 6. Level Shift Circuit (LM741-Op Amp) Captured Using NI Multisim v12.0

As stated earlier the output voltage range of the IQ demodulator is +/- 400 mV, however the analog to digital converters can only read positive voltages in the range of 0 to 3.3V. The solution to this problem is to use a level shift circuit. The level shift circuit is designed to convert input voltages within the range of +/- 400mV to the range of 0 to 3.3V. This circuit was designed to have a gain of 4.125 (12.3 dB), which is the desired range of output 3.3V divided by the input range 800mV. The equations for the gain are shown below:

$$A = \frac{R4}{R1} * \frac{(R1 + R2)}{(R3 + R4)}$$

Equation 5: Gain for level shift op amp circuit

$$A_{Offset} = \frac{(R2 + R1)}{R1} * \frac{R3}{(R3 + R4)}$$

Equation 6: Gain of the offset voltage

The overall goal of the analysis for the receive chain was to calculate the noise power received from the reflections off of the target. This value is with respect to the analog to digital converters which act as the receiver for the entire radar system. In order to calculate this value

the noise figure for the entire receive chain was needed as well as the gain. Calculating the gain was straightforward the value was 51.3 dB. However for the entire noise figure the analysis required more thought. In order to calculate the chain noise figure a cascade model was used. This involved calculating the noise figure of the chain as each additional component was added to the chain. At the end of the last component which was the IQ demodulator the noise figure for the entire chain was equal to that value calculated. The equations are shown below:

$$nf_N\,(\text{magnitude}) = nf_1 + \frac{nf_2 - 1}{gain_1} + \ldots + \frac{nf_N - 1}{gain_1 * \ldots * gain_{N-1}}$$

Equation 7: Cascaded Noise Figure

$$nt_N\,(\text{magnitude}) = nt_1 + \frac{nt_2 - 1}{gain_1} + \ldots + \frac{nt_N - 1}{gain_1 * \ldots * gain_{N-1}}$$

Equation 8: Cascaded Noise Temperature

$$N\ (\text{dBm}) = N_n\ (\text{dB/Hz}) + G_{Rx}\ (\text{dB}) + NF\ (\text{dB}) + B_L\ (\text{dB})$$

Equation 9: Noise Power at the Receiver

$N_{n:}$ Thermal noise due to nature = -174dBm/Hz
G_{Rx}: Gain of the receive signal chain = 51.3 (dB)
NF: Noise figure of the receive chain using the cascaded approach = 12.9 (dB)
B_L: Limiting bandwidth of receiver = 275 MHz

When calculating the cascaded noise figure it was noticeable that after the first low noise amplifier the cascaded noise figure did not change much. This was due to the relatively high gain of the low noise amplifier in comparison to the other components in the chain. After performing the calculations the noise figure for the receive chain was 19.5 (magnitude) or 12.9 dB.

The next step in the calculations was to calculate the noise power at the receiver. This is shown in equation 9 above. After inputting the values, the noise power calculated at the receiver was -26.6 dBm (2.188e-6 W).

2.2.5 Signal to Noise Ratio

$$\frac{S}{N} = \frac{Received\ Power\ at\ Receiver}{\text{Noise Power at Receiver}}$$

Equation 10: Signal to Noise Ratio

$$P_r = \frac{P_t G_t G_r \sigma}{4\pi R^2}\ (\text{mW}) = 10 * \log\left(\frac{P_t G_t G_r \sigma}{4\pi R^2}\right)\ (\text{dBm})$$

Equation 11: Received Power

The signal to noise ratio (SNR) is the measure of the ability of a radar to detect a target at a distance away from the radar. This equation is a way in which the target, the radar, the range of the target and the properties of the medium through which the signal will travel are related

mathematically. The physical properties of the target that affect the SNR is the target's radar cross section. The radar cross section is the measure of how detectable the object is by a radar. In the analysis the radar cross section was calculated for a trihedral corner reflector. This shape was chosen by the customer; it would have been much simpler to use a sphere however the trihedral was chosen. The lengths of its sides are 0.0508 meters. The equation used to calculate the maximum radar cross section this trihedral is shown below:

$$\sigma_{\max} = \frac{12\pi L^4}{\lambda^2}(m^2) = 10*\log(\frac{12\pi L^4}{\lambda^2}) \text{ (dBsm)}$$

Equation 12: Maximum radar cross section of a trihedral corner reflector

The value solved for the radar cross section used in the SNR equation was -5.5446 dBsm. The radar characteristics that were used in the SNR equation included the power transmitted and the characteristics of the antenna aperture. As explained before the transmitted power (P_t) was determined by the components in the signal transmission chain and the value calculated was 24.5 dBm (281 mW). The properties of the antenna aperture that are used in this equation are the gain of both transmit and receive antennas. The gain for the transmit and receive antennas are 17 dB.

The signal to noise ratio as shown in equation XX uses the signal power at the input of the receiver which in this case is the output power from the IQ demodulator (5dBm). The SNR equation also uses the noise power at the input of the receiver which was calculated using equation XX shown above (-25.4dBm). Since these values are calculated in dBm, SNR (dB) = S(dBm) – N(dBm), which results in a value of 30.4 dB.

2.2.6 Field-Programmable Gate Array (FPGA)

The FPGA is responsible for relaying information to the personal computer (PC), voltage controlled oscillator (VCO), analog-to-digital converters (A/D), and switches. Utilizing an FPGA, the team can easily make necessary adjustments to the radar system, specifically adjusting the timing of each switch in the design. An FPGA is re-programmable device that allows its users to reconfigure hardware to for new applications. The selected FPGA board for this design will be the Digilent Nexys 3. As the electronic controller of the SAR Imager system, it is the most important and complicated device in the system.

2.2.6.1 Hardware Design

The most useful peripherals on the FPGA that will be used are the PMOD port, VGA port, and the USB port. The PMOD port allows for an Analog to Digital converter that is made specifically by the company Digilent to have guaranteed compatibility with the FPGA, while the VGA port will be used to connect the VGA to the VGA display. The USB port will allow the PC to be plugged directly into the FPGA for simplicity of the overall setup. The reason why a high clock ratio of 100MHz was desirable was because a 100 MHz clock has a period of 10 ns which could thereby allow the switching of components every 10 ns. Any time something is switched between on and off, it does not happen instantaneously as there is a rise time and settling time. If the rise time is really sharp, this will cause the load to have some ringing. By

having a larger off time for the pulse and a higher clock which causes less ringing from the rise time, the timing for the system can be more exact. Because of this, the overall switching speed for the system will be a combination of rising time, settling time, component delay and external factors (which include electrical interference, cabling, etc.).

Figure 7 is a block diagram of the FPGA that consists of what components the FPGA talks to directly in the system. Comments are denoted next to the arrows describing either what relationship the device and the FPGA have, or the signal that is used by the FPGA to control the device.

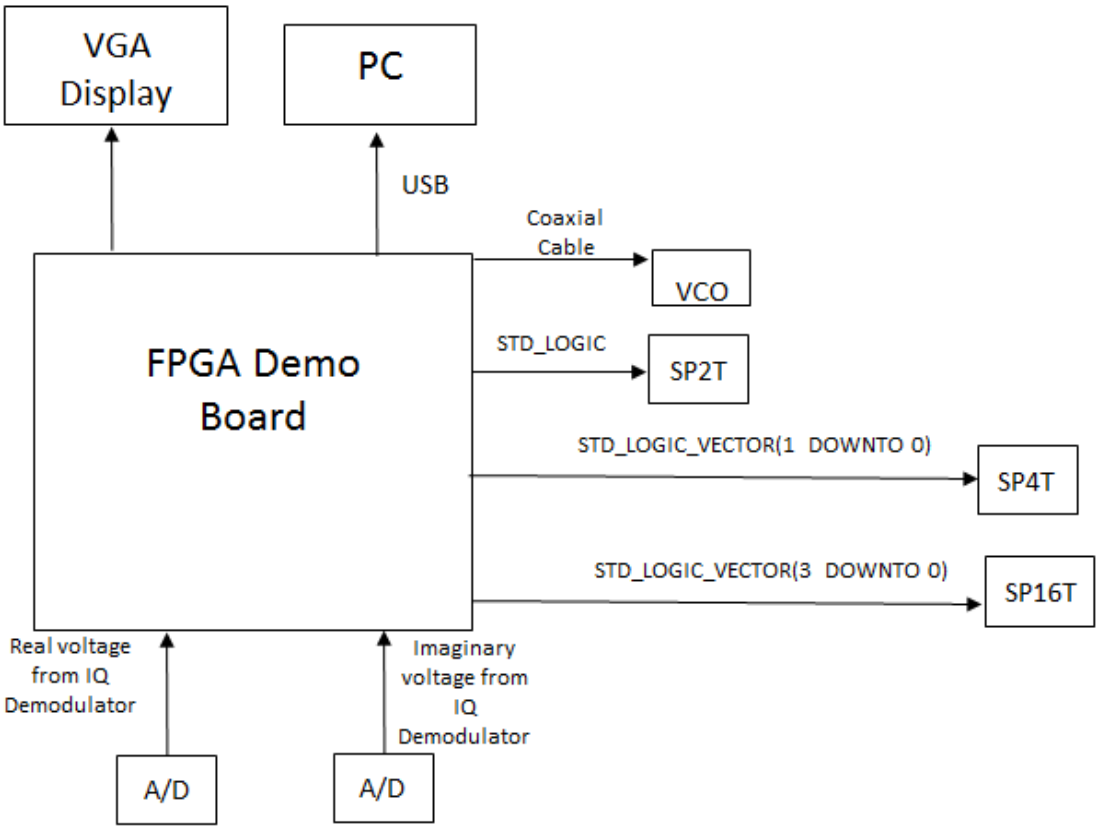

Figure 7. FPGA Block Diagram

Notes:

1. Signal of type STD_LOGIC_VECTOR was used for the signal going to the SP4T and SP16T switch to take into account the compatibility of the logic of the switches. Since SP4T has four different combinations, this needs a two bit number to take the four different combinations (00, 01, 10, 11). The same logic goes for the SP16T switch except it needs four bits instead of two to handle 16 combinations.

2. Signal of type STD_LOGIC was used for SPDT for simplicity. In reality, the only outcomes for logic the switch can handle is 0 or 1, so signal of type BIT could be used as well.

3. The VCO used for this project is connected directly via a Coaxial cable which is used to transmit the reference voltage. This coaxial cable can be directly plugged into the FPGA.

4. The USB port connects the PC directly to the FPGA to allow frequency to be set. The USB port is also used to control the frequency of the RF system since this would allow for simplification of design by not having a Digital to Analog converter. The new updated block diagram of the system shows this.

2.2.6.2 Timing Diagram

Figure 8 is a preemptive timing diagram which shows the theoretical timing between the switches. This is not the exact timing that will be used for the system because in real life there are external factors which cause delay. Some of these delays include switching time of components, cabling, settling, and electrical interference to name a few. The preemptive timing diagram below is just to elaborate the relationship between the switches, clock, and the output pulse. For the next phase in the system design when actual code is written, delay will be taken into consideration by testing the code.

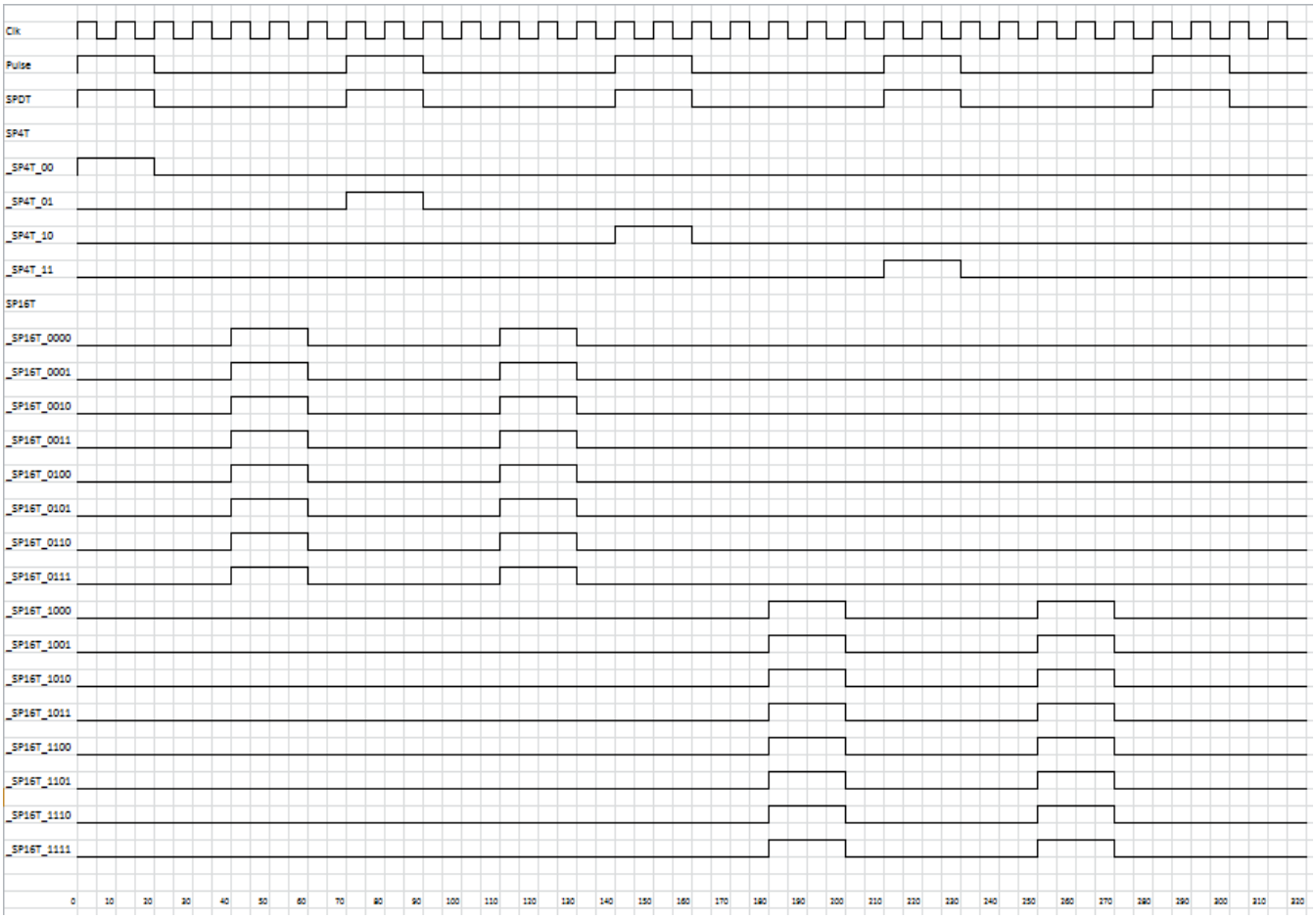

Figure 8. Preemptive Timing Diagram

Notes:

1. The signal Clk is the clock from the FPGA, which is 100MHz which turns out to be 10ns from rise time to rise time. This will use the pin V10.

2. The signal pulse is the output signal from the transmit antennas. When it is logic 1 it is emitting the pulse and logic 0 means it is not emitting a pulse. The signal period was chosen to be 70ns in total, with the first 20 ns being when the signal pulse is on and the rest of the 50 ns when the pulse is off. This is because since the target from the transmit antennas is 20 feet away, the speed of a radio wave travels at 1 nano foot per second in air. This yields the first 20ns for the entire signal to be output and the beginning of the signal that is output after 20 ns reaches the target at 20 feet away. The next 40 ns after the entire pulse is transmitted is for the part of the signal that has hit the target after the first 20 ns to hit the receiver and for the part of the signal that is just leaving the transmitter after 20 ns to hit the receiver. The rest of the 10 ns for the period of pulse are for other factors such as settling, switching, and hardware/software delay. When testing occurs, more or less time may be added for the portion of when the pulse is off to match physical factors of implementing the system.

3. The signal SPDT controls the transmit and receive paths. When the signal SPDT is logic 1, the system is in transmit mode and when the signal is logic 0, the system is in receive mode. The reason for this choice for logic 1 and logic 0 is because of the inherent truth table of the SPDT switch that was chosen for the system. The switching speed of the SPDT switch needs to be the fastest of all the switches because it needs to rapidly switch between transmit and receive mode before any of the other switches takes effect. In the above timing diagram settling and component delay is not taken into consideration, but it will be a noticeable factor in empirical testing.

4. The signal SP4T controls the four transmit antennas. SP4T has four combinations that have each combination controlling a specific antenna by each possible combination of two binary digits. Note that at any point the transmit antennas will only be logic 1 when in transmit mode. In the above timing diagram settling and component delay is not taken into consideration, but it will be a noticeable factor in empirical testing.

5. The signal SP16T controls the sixteen receive antennas. SP16T has sixteen combinations that have each combination controlling a specific antenna by each possible combination of four binary digits. Note that at any point the transmit antennas will only be logic 1 when in receive mode. In the above timing diagram delay is taken into consideration by adding the extra 10 ns in the off time for the signal pulse. Note that not all of the eight antennas that are receiving are turned on at the same time, even though it looks like that in the timing diagram. Since the antennas are only separated by 3 inches, the delay component of the signal SP16T would be 0.25 ns since the signal would travel a nanosecond per foot. This yields the very small delay in between the components of the SP16T signal which are too small to see in the preemptive timing diagram but are taken into account for the timing of the switches.

2.2.6.3 Coding Sequence

To separate the sequence of coding milestones for this project, the code design was separated into blocks. Each block plays a specific purpose of importance for the completion of the project. Figure 9 is a block diagram consisting of the main blocks of code that will need to be completed for this project. A description of each of these blocks is given below, and each of them is numbered as well. Note that the number that is assigned to them does not equate to how important the block is.

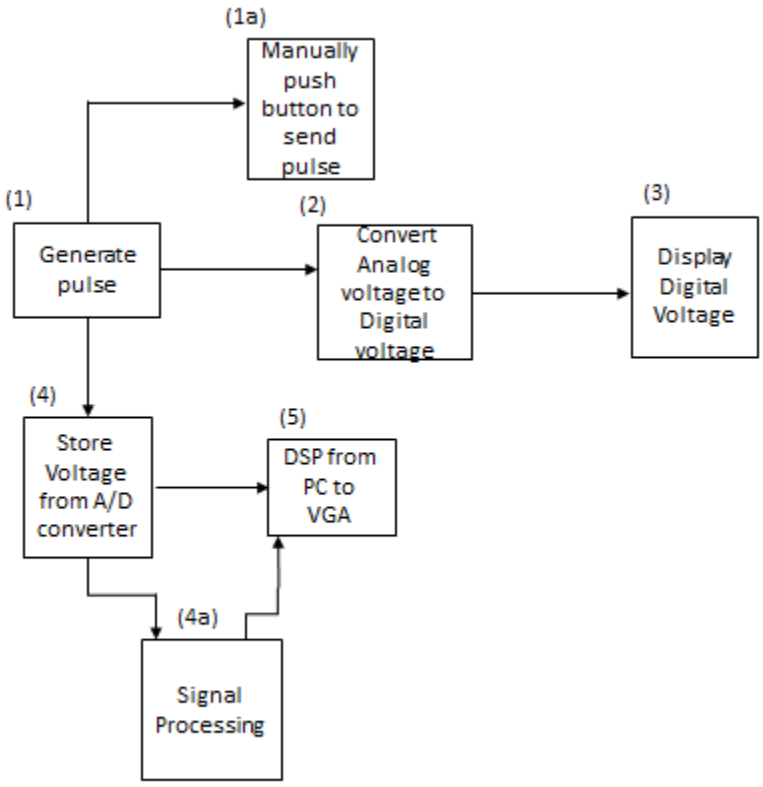

Figure 9. Coding Procedure Block Diagram

Block Diagram Descriptions (Number References Specified Block):

1) Code will be written to generate pulses for the timing of the SPDT, SP4T, and SP16T switches.

1a) Code will be written to manually flip a switch on the board that will send out the pulse. The purpose of this step is to check the functionality of the FPGA in regards to generating a signal. The exact button on the board that will be used is BTNL and the pin is C4. Note that there were many other switches that could have been used, so a generic switch on the board was just picked.

2) Code will be written to convert Analog voltage to Digital voltage. The A/D converter will take voltages ranging from 0 to 3.3 V from the level shifter circuit and convert that information in a 12 bit word.

3) After the code is converted from Analog Voltage to Digital voltage to a 12 bit word, the voltage will be displayed on the 7 segment display of the FPGA. As the analog voltage input changes, the display of the value on the hex display would change as well. This would verify the operation of the code for the Analog to Digital conversion. The pins used for the seven segment display on the FPGA would be pins CA, CB, CC, CD, CE, CF, CG, DP, AN3, AN2, AN1, and AN0.

4) The data that is the result of the analog to digital conversion will be stored onto the FPGA. This will allow for the data to be worked on via code that is written from the signal processing, or the data will be sent to the PC via the USB.

4a) This step is an intermediary step that will include having code written for the signal processing of the data in VHDL. This step will only be taken if signal processing is not able to be done on the PC using a program such as LabVIEW.

5) Code will be written that receives the signal processing from the PC (or on the FPGA) and outputs it to the VGA display. Slider switches would be used to generate a digital word that is proportional to what pixels would get activated on the display. This would be to show the functionality of the PC in regards to how the signal processing results come out. The slider switches that would be used for this portion of code would be SW0, SW1, SW1, SW2, SW3, SW4, SW5, SW6, and SW7. The respected pins for the said buttons are T10, T9, V9, M8, N8, U8, V8, and T5.

2.3 Antenna Design

2.3.1 Antenna Hardware

The necessary hardware for the antenna design must be able to handle X-band frequencies and propagate a signal with a beamwidth that will cover a scene extent of at least 30 inches from a distance of 20 feet away. The highest gain value to create the precise beamwidth is 26 dBi. Attached to each horn antenna will be a Waveguide-to-coaxial adapter (iso-adapters), which will convert analog signal and transform it to become electromagnetic waves ready for propagation. Selecting the proper hardware is critical to confirm the X-Band impedance matching process occurring within the horn antennas. The design will utilize the X-Band horn antennas from Advanced Receiver and WR90 Waveguide Isolator from TestParts.com.

2.3.1.1 MA86551 X-Band Horn Antennas

The MA86551 X-Band horn antennas are from Advanced Receiver. Each horn has a gain level of 17 dBi that will create a beamwidth of 25°, covering a scene extent of 9 feet squared, which will cover the minimum scene extent of 30 inches squared. The antennas will

mate with a WR90 iso-adapter and has a UG-39/U flange. WR90 represents horns or transmission lines functioning at X-Band frequencies, and the UG-39/U signifies the horn antenna will be brass.

2.3.1.1.1 Specifications

Table 5 is the MA86551 X-Band horn antenna's data sheet, and Figure 10 is the actual horn antenna the design will be utilizing. The dimensions for the MA86551 horn antennas are list in Table 2 and illustrated in Figure 11.

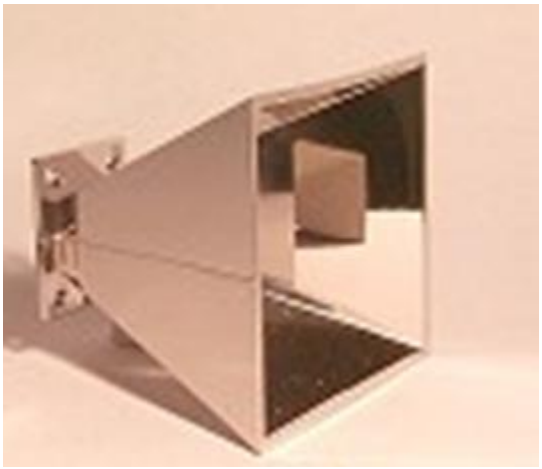

Figure 10: MA86551 X-Band Horn Antenna

Table 5. MA86551 Horn Antenna Data Sheet

Horn Antenna Specifications Data Sheet	
Center Frequency	10.525 GHz
Frequency Range	8 – 12.4 GHz
Nominal Gain	17 dBi
H-Plane (Azimuth) Beamwidth	25°
E-Plane (Elevation) Beamwidth	25°
Scene Extent	9' x 9'
RF Connection	UG-39/U
Price	$20.00 per antenna

Table 6: Horn Antenna Dimensions

MA86551 Horn Antenna Dimensions	
Length	3 in.
Width	3 in.
Height	3.688 in.
Waveguide Entry	1.280 in.
Flange Size	1.625 in.

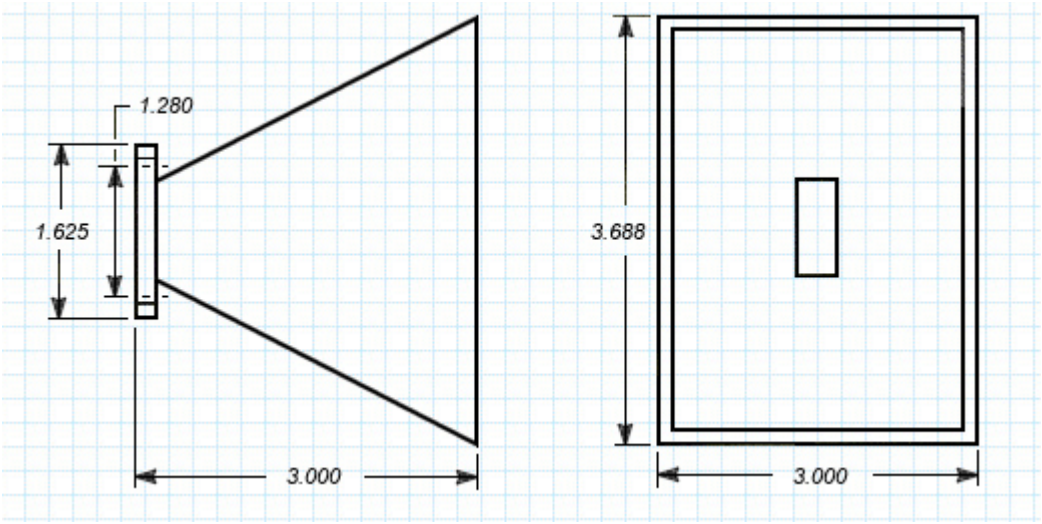

Figure 11: MA86551 Horn Antenna Dimensions

2.3.1.2 Waveguide-to-Coaxial Iso-Adapter

The WR90 Waveguide Iso-Adapter from TestParts.com covers the X-Band frequency range and will be sufficient for transforming the analog signal from a coaxial cable to waveguide and eventually out the horn antenna. The adapter will also be able to perform the transformation in reverse, converting a received electromagnetic signal wave into an analog signal. Each horn antenna is required to be connected to an iso-adapter. Table 7 lists the specifications for the iso-adapter, and Figure 12 is the actual WR90 Waveguide Iso-Adapter.

Table 7: Waveguide Isolator Specifications Sheet

WR90 Waveguide Isolator X-Band Data Sheet	
Frequency Range	8.2 – 12.4 GHz
RF Connection	WR90
Price	$79.95

Figure 12: WR90 Waveguide Iso-Adapter

2.3.2 Antenna Design Principles

Having the T-shaped design with two linear antenna arrays; the transmit antennas spaced 3λ from the outer receive antennas; and the receive antennas spaced 6λ from their neighboring receive antennas was conceptually and theoretically determined based on various antenna theory guidelines. One linear antenna array aperture covers one dimension of a scene. The horizontal array aperture covers the azimuth dimension of the scene, and the vertical array aperture covers the elevation dimension of the scene. Thus, the two array aperture crossing will

allow two dimensional scanning of a scene. Due to the low gain level of the antennas and large beamwidths, angling the horn antennas toward the scene extent is unnecessary.

2.3.2.1 Antenna Spacing

For each array aperture, eight receive antennas will be linearly aligned, spaced six inches apart from each antenna's center point. A transmit antenna will be placed on both ends of the array aperture, spaced three inches from the neighboring receive antenna. Figure 13 illustrates the design of one linear array aperture. The spacing and the antenna configuration will create 16 phase centers for one array aperture. Each phase center will be 3λ apart from each other.

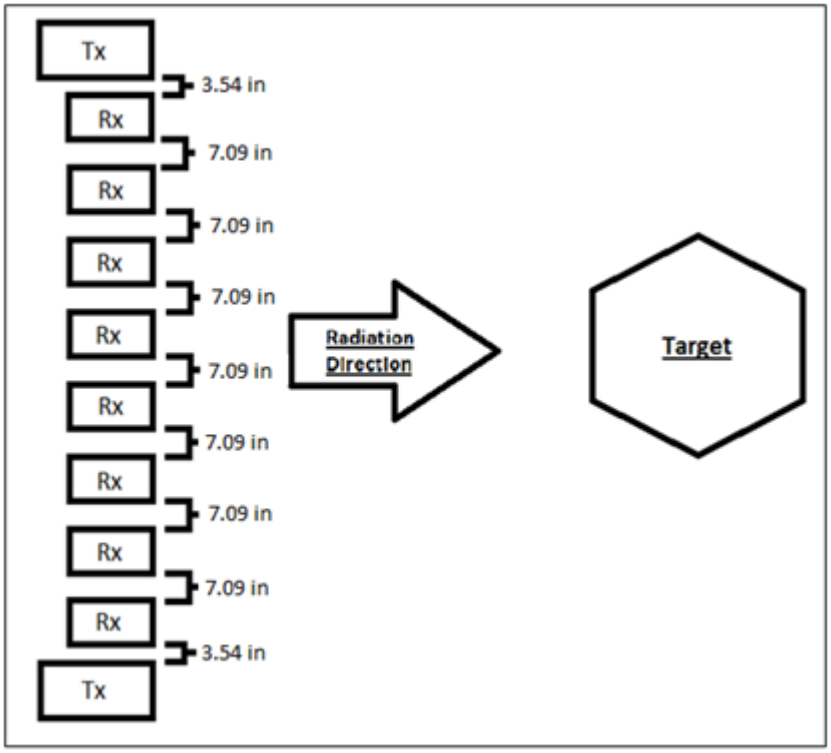

Figure 13. One Antenna Aperture Design

2.3.2.2 Phase Centers

The construction of one antenna aperture creates sixteen phase centers – a phase center is a maximum absorbance point of a reflected signal and is located between one transmit and one receive horn antenna. Each transmit horn antenna is responsible for eight phase centers. Two transmit antennas on both sides of an antenna aperture creates 16 phase centers per array aperture. The phase centers are spaced 3λ away from each other. The spacing between phase centers is calculated to prevent the main lobe from an antenna aperture to scan the size of the scene extent without having excessive grating lobes entering the scene – a grating lobe is radiation directed at a different angle than the main lobe and is similar in strength as the main lobe. If grating lobes enter the scene, receive antennas will gather multiple return signals and

cause confusion and errors when processing the data. Figure 14 illustrates the phase center locations on one of the antenna array apertures. The red and blue arrows represent the phase centers in correlation to their same colored transmit antenna. Each antenna aperture has the same amount phase centers and at the same locations, theoretically. Thus, Figure 14 represents both the azimuth and elevation antenna arrays.

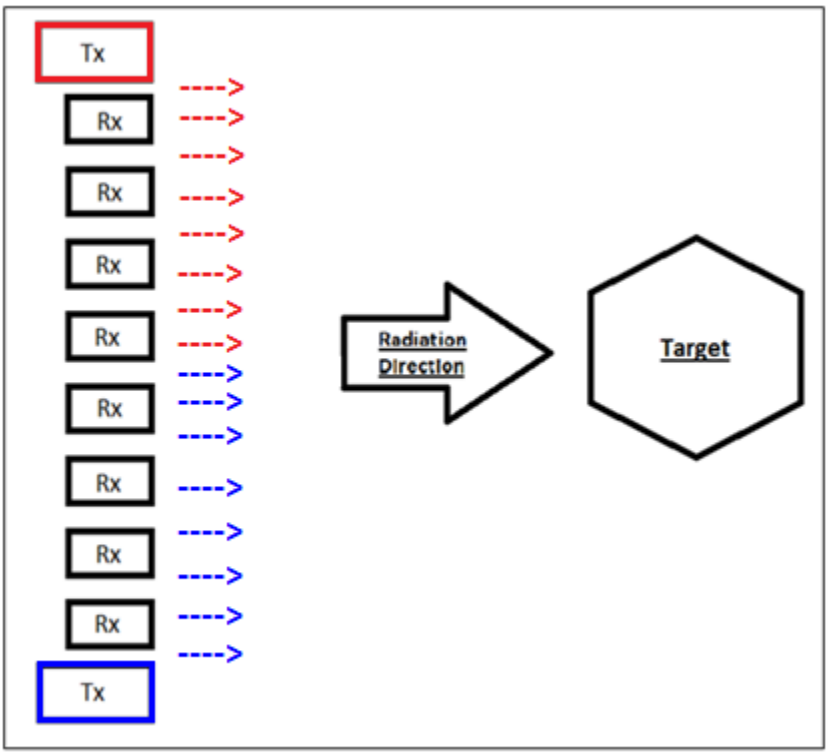

Figure 14. Phase Center Illustration

2.3.2.3 Linear Antenna Array Radiation Patterns

The arrangement of the horn antennas in a linear array and the 3λ spacing between phase centers creates a main lobe with grating lobes 20 degrees spaced from the main lobe. Justifying the 3λ spacing required generating the total radiation pattern equation based on multiplying the element factor and array factor equations. Once the total radiation pattern equation is complete, the next step is to plot the equation to simulate the beams originating from the antenna array. Once the main lobe and grating lobes are angled far enough apart based on the simulation plots, the distance is justified. For this design the 3λ is a workable distance and isolates the main lobe.

2.3.2.3.1 Element Factor

The element factor for both antenna arrays does not account for the amount of elements in the array – elements are the phase centers, which in the array there are 16 phase centers. The element factor's plot appears like a half oval and is similar to the propagation output of only one horn antenna. Axes on the plot are the element factor representing the y-axis and the zenith angle representing the x-axis. The zenith angle (θ) is the unknown variable

and will be plotted from zero to 90 degrees. Validated by plots in Figure 15, the element factor demonstrates where the strong and weak points are located in the propagation shape. When the zenith angle decreases or increases by 90 degrees, the signal becomes weaker and eventually vanishes. Equation 13 signifies the element factor, and Table 8 are the variable values. Figure 15 illustrates two different propagation plots that simulate one of the linear array's element factor.

$$EF = \sqrt{\cos(\theta)}$$

Equation 13: Element Factor

Table 8: Element Factor Variables

Element Factor Variables		
Description	***Variable***	***Value***
Zenith Angle Range	Θ	0-240°

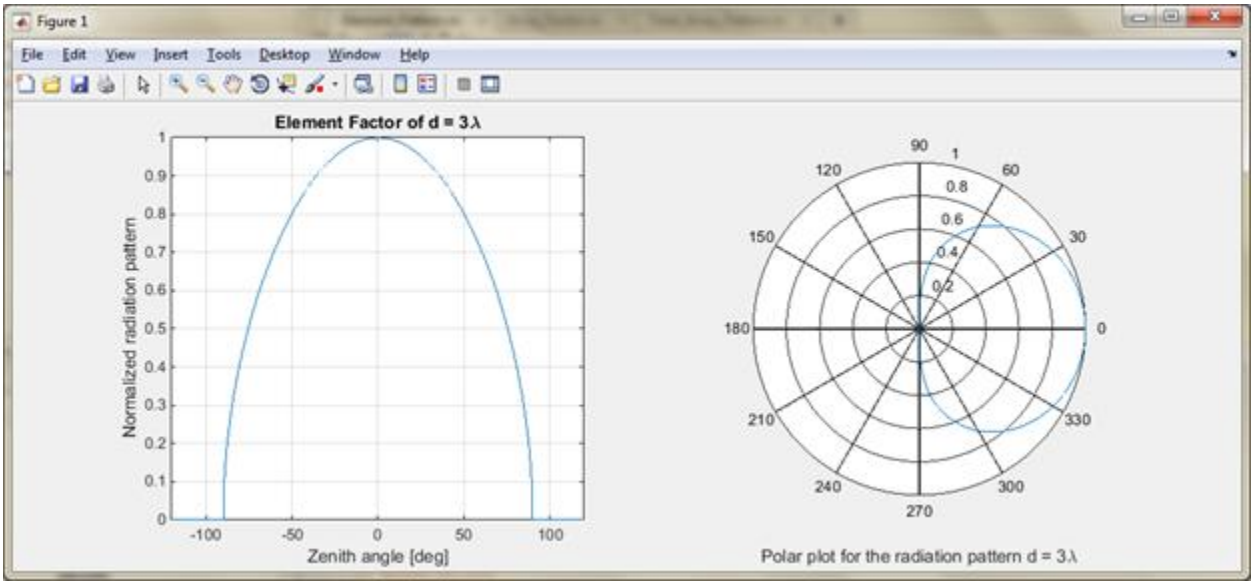

Figure 15. Element Factor Simulation Plots

2.3.2.3.2 Array Factor

The array factor is the propagation effect when implementing multiple antennas in an array. The equation takes in the amount of phase centers (N), distance between antennas (d), a 'k' constant (k), and the zenith angle (θ). Table 9 specifies the values of each variable. The array factor's plots in Figure 16 simulate the distances between the main lobe and excessive grating lobes at different angles. However, the array factor equation does account for the

signal strength as the angles from the antenna array increase or decrease. For equation 14, 10 horn antennas are inputted. The zenith angle ranges zero to 90 degrees.

$$(AF)_N = \left| \frac{1}{N} \frac{\sin\left(\frac{Nkd}{2}\cos(\theta)\right)}{\sin\left(\frac{kd}{2}\cos(\theta)\right)} \right|$$

Equation 14: Array Factor Equation

Table 9: Array Factor Variables

Array Factor Variables		
Description	***Variable***	***Value***
Antenna Spacing	d	3λ
No. of Elements/Phase Centers	N	16
Wavelength	λ	0.03 m
k-constant = $\frac{2\pi}{\lambda}$	k	209.44
Zenith Angle Range	θ	0-90°

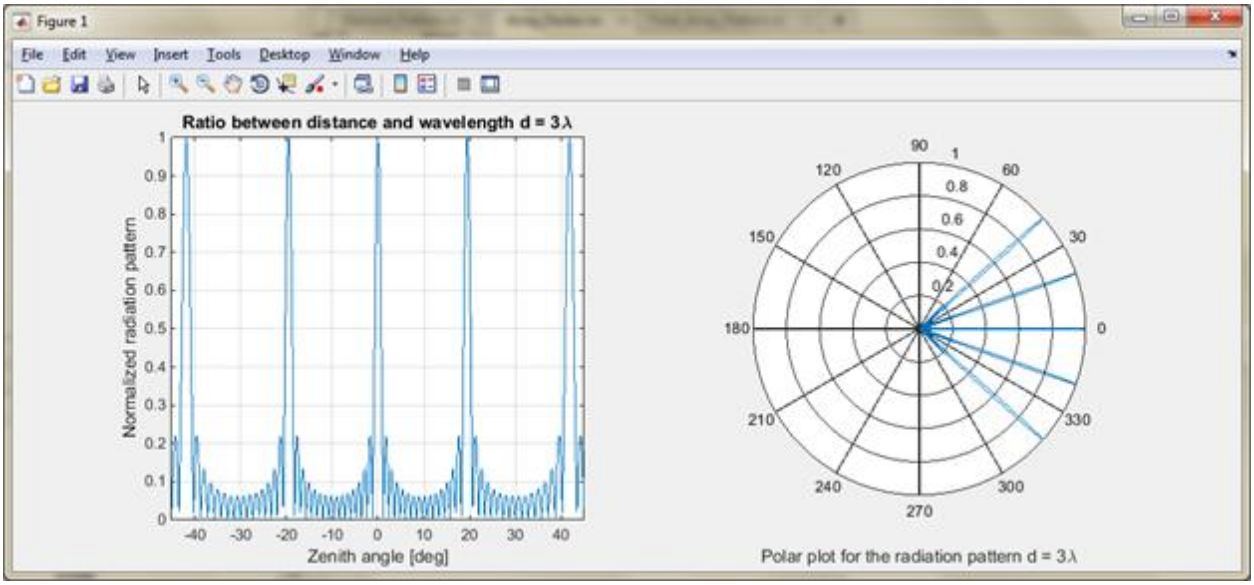

Figure 16. Array Factor Simulation Plots

2.3.2.3.3 Total Radiation Pattern

The total radiation pattern equation is both the element factor and array factor multiplied together. The plots in Figure 17 demonstrate the distances between the main lobe and grating lobes, but also illustrates how to the grating lobes weaken as the zenith angle

decreases or increase. The simulation plots of the total radiation pattern validate that the spacing of phase centers at 3λ will allow the main lobe of the linear antenna array to scan the scene without excessive grating lobes also propagating onto the scene. Equation 15 represents the total array radiation, and Table 10 specifies the variable values, which are the same from the element factor and array factor.

$$TAP = EF \cdot AF = (AF)_N = \left| \frac{1}{N} \frac{\sin\left(\frac{Nkd}{2}\cos(\theta)\right)}{\sin\left(\frac{kd}{2}\cos(\theta)\right)} \right| \cdot \sqrt{\cos(\theta)}$$

Equation 15: Total Array Radiation (TAP) Equation

Table 10: Total Radiation Pattern Variables

Total Radiation Pattern Variables		
Description	***Variable***	***Value***
Antenna Spacing	d	3λ
No. of Elements/Phase Centers	N	16
Wavelength	λ	0.03 m
k-constant = $\frac{2\pi}{\lambda}$	k	209.44
Zenith Angle Range	θ	0-90°

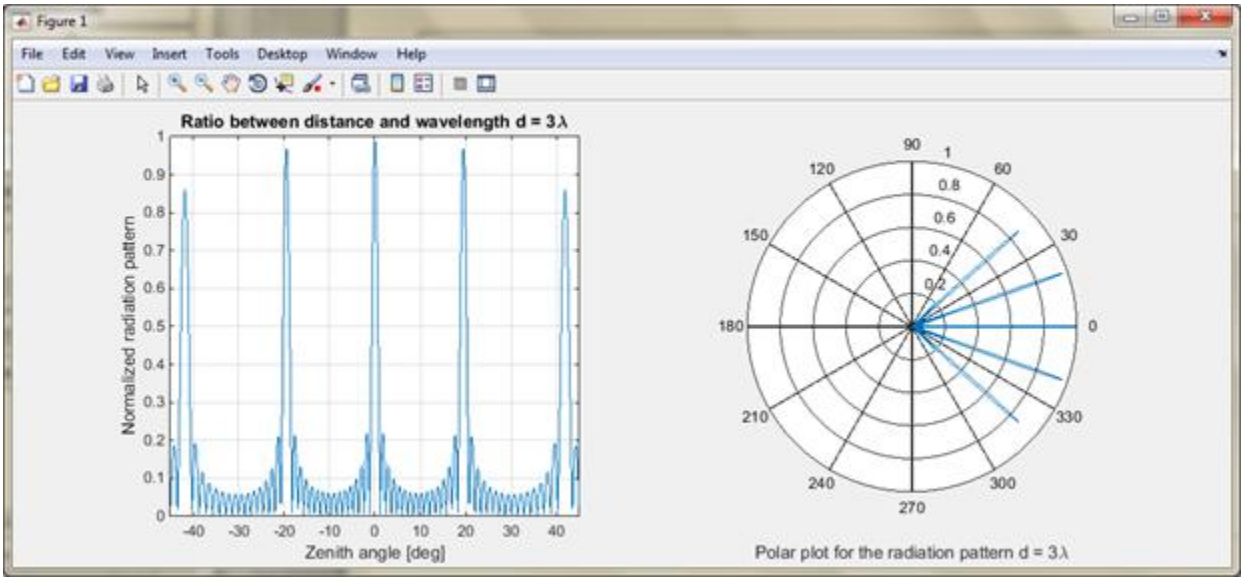

Figure 17. Total Radiation Simulation Plots

2.4 Antenna Structure Design

2.4.1 Antenna Structure

The horn antenna structure will be made of an aluminum based metal for light weight and machinability. The structure will be made in separate sections to piece together because of its width and height being 5.5 ft x 5.5 ft. The goal is to have four separate quadrants which will be connected together with a divider to allow enough space in between quadrants for the horn antennas to be placed. Below in Figure 18 shows one quadrant panel and one connector/divider for two quadrant panels.

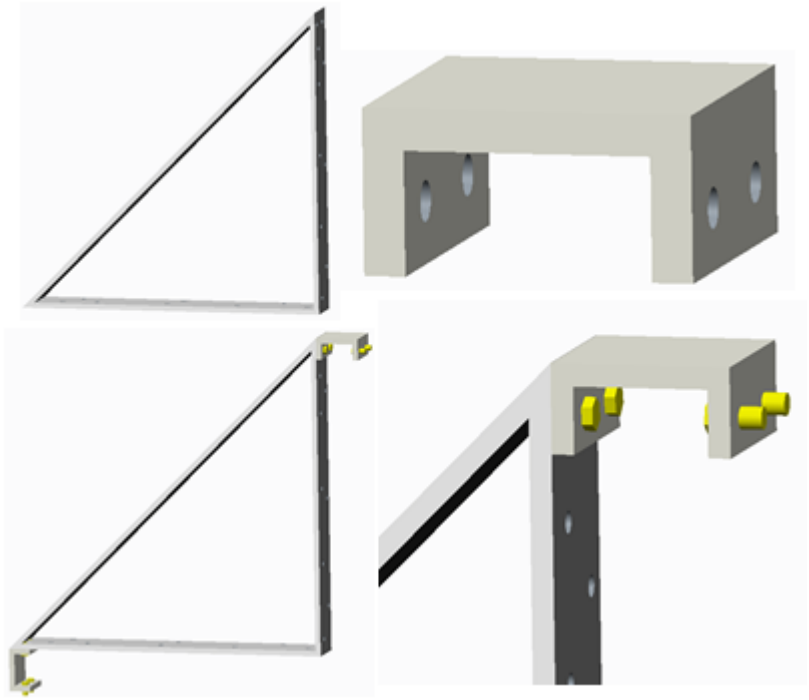

Figure 18. 3-D Model of Quadrant Panel, Connector/Divider, and Screws

The quadrants panels will be connected to the connector/divider with 0.5 in diameter screws so no bolts will be required. The hole to insert the screw will be threaded. The horn antennas will be aligned along the open space between quadrants with the correct distances between each receiving to receiving horn 7.09 in and transmit to receiving 3.54 in. The horn antennas will have two 1 in diameter bolts placed along the center of gravity from the horn and wave guide adapter combo. The bolts will attach to the horns with industrial Velcro for ease of taking the horns off of the structure. Below in Figure 19 is a rough model showing how the Velcro would be attached.

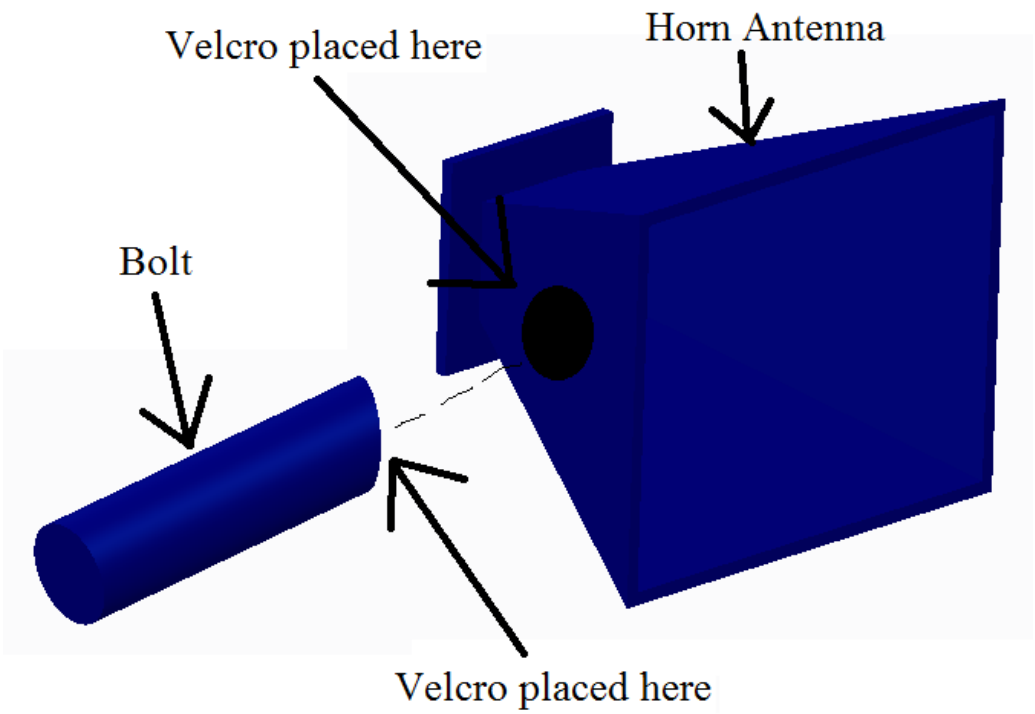

Figure 19. 3-D Model of Horn Antenna Explaining Velcro Placement

The horn antennas with the Velcro attached bolts will be bolted onto the quadrants panels with four nuts, two for each bolt, as shown in Figure 20.

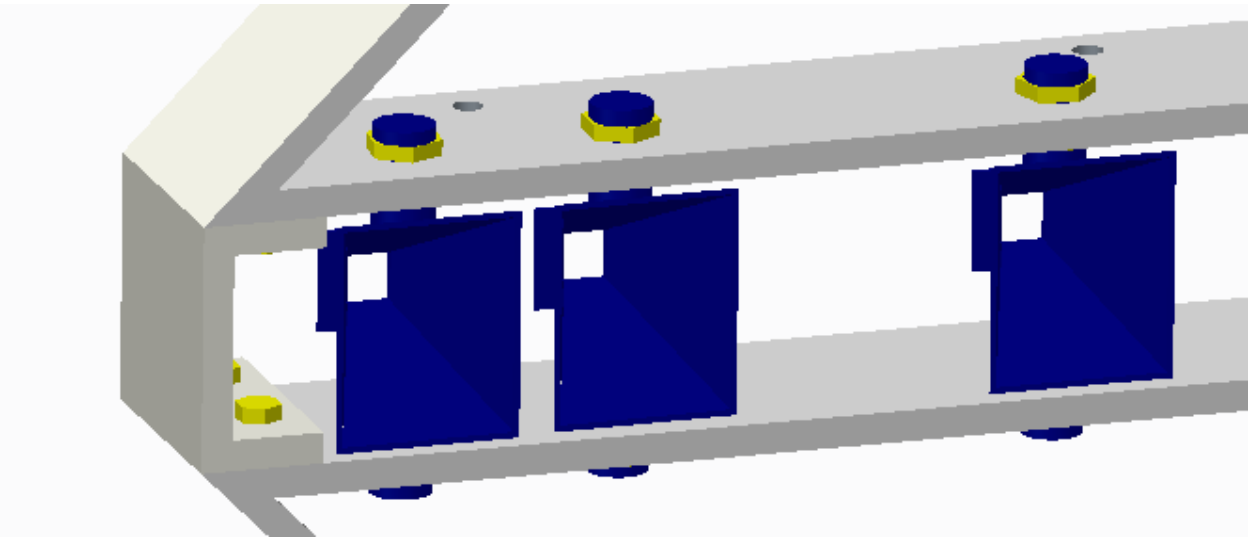

Figure 20. 3-D Model Showing Horn Placement on Structure

The horns will be flush with the front of the structure so no interference could come from the aluminum metal and disrupt the signal. Four horn covers will be bolted onto the back of the structure to cover the horns and the wires running to the horns. The covers will also add extra support for the structure. Below in Figure 21 shows the full design of the horn structure without the stand and component box.

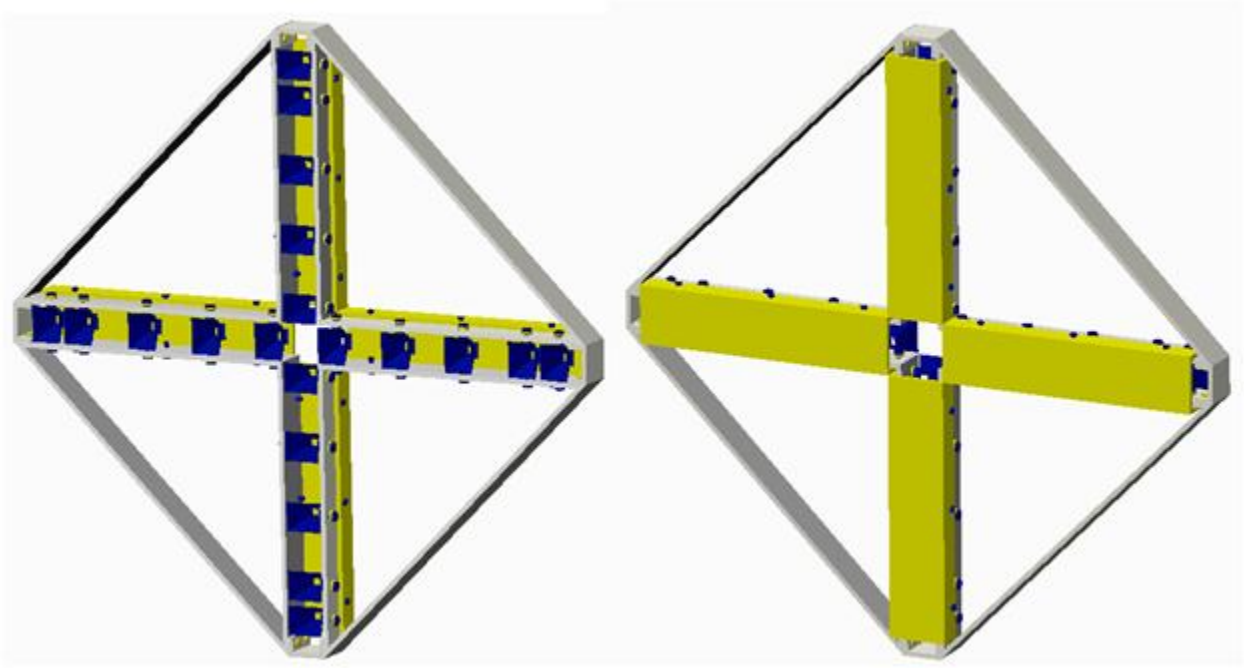

Figure 21. 3-D Model of the Horn Antenna Structure without Stand and Component Box

2.4.2 Antenna Structure Stand

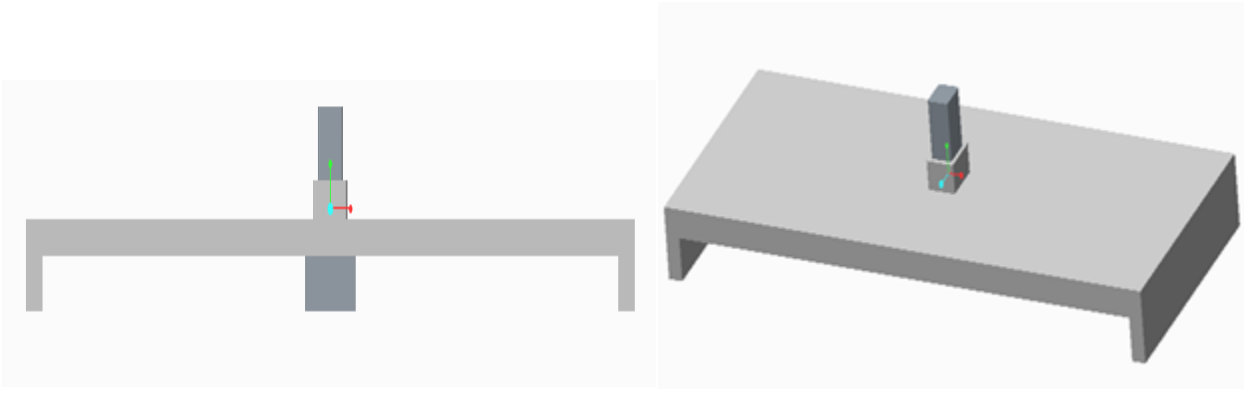

Figure 22: Antenna Stand Structure

In Figure 22, the stand for the structure can be seen. After much analysis, a rectangle base stand will support the weight of the antenna structure on all sides. The stand will be connected with a pin joint that is rectangular and ideal for the rigidity needed to keep the structure fixed in

the desired position. The male end of the joint is 4 inches with a stopper 2 inches up from the surface of the base. The dimensions of the joint are 3x3 inches. The matching female end will be on the bottom of the antenna structure with identical measurements. The stand will be aluminum and efficiently sturdy as expected. The base will have a supporting 3rd leg to ensure the weight is evenly distributed.

2.4.3 Antenna Structure Electrical Component Box

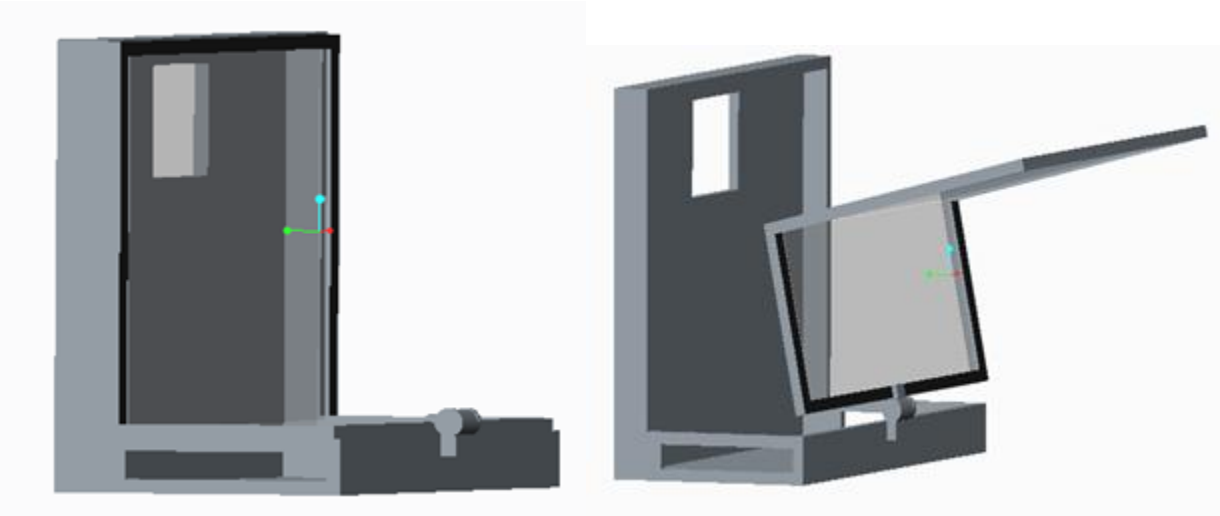

Figure 23: Electric Component Box

The electrical components must have a component box that is convenient to the user and the structure. Figure 23 above shows the component box in both the open and closed position. At the front of the component box, there will be a hinge place to create a rotation about. Whenever the components need to be worked on, the lid can be easily opened. The lid consist of many advantages: clear window to view components at all time and a door rotates open and forms a stand for the user to place components on. The window of the component box will be scratch proof glass. This glass is referenced as gorilla glass, used widely for protection and durability. This is ideal for the component box because the electrical components must be secured and protected at all times. Also in Figure 23, you can see cuts into the component box. From the antenna to the PC, there will be numerous wires need to travel. The square cut out toward the top of the component box will allow access to the wires that will be traveling to each antenna. The rectangle cut outs on the side allows for a convenient PC connection to the VGA input and USB input. The material of the component box will be aluminum for durability of environmental effects with a lining of wood to allow ease of electrical components to be screwed to the box. Aluminum has a tough surface and is very resilient. The component box will be attached through slits that are cut into the component box. The back plate of the structure will have arms that extend out horizontally and are pushed along the hole for a confirmed fit.

The electrical components will be placed in the component box by either a screw that is provided for the appropriate parts. If the component does not supply screw access then brackets

to hold down the component will be purchased. Each bracket will be different to provide for a secure fit without disturbing the function of the component. Below in Figure 24, The Structure with all the parts can be viewed for clarification. As you can see, the female joint for the stand come out of the bottom of the structure. This joint will be bolted to the structure, similarly to the three other caps located on each side of the diamond.

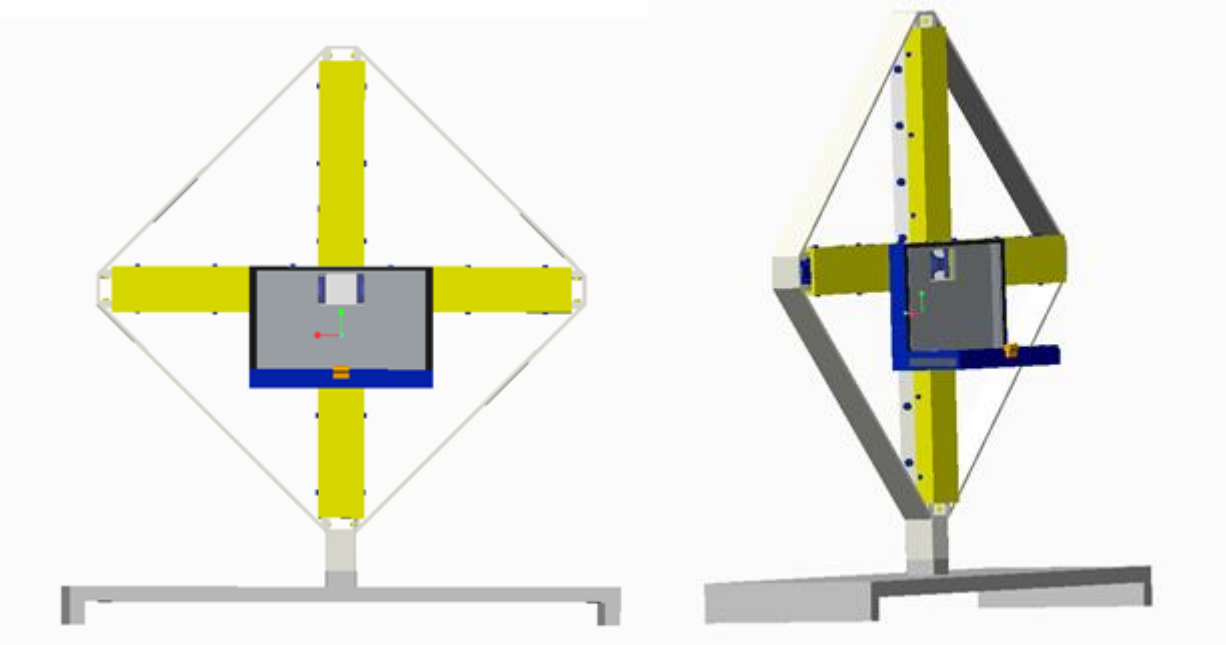

Figure 24: Complete Antenna Structure Design

2.5 Power System

The power system for the radar system will consist of power supplies that will be used to power the FPGA board and the components used in this system. The components that require input power are the voltage-controlled oscillator (VCO), field programmable gate array (FPGA) board, analog-to-digital (A-to-D) converters, single-pole double-throw (SPDT) switches, single-pole 4-throw (SP4T) switch, single-pole 16-throw (SP16T) switch, IQ demodulator, frequency multipliers, wideband amplifier, low noise amplifier (LNA), and power amplifiers. The task of the power supply is to provide steady power to the components in the system.

Table 11. Input Voltage and Current for each Component

Part Name	$+V_{supply}\ (V)$	$+I_{supply}\ (mA)$	$-V_{supply}\ (V)$	$-I_{supply}\ (mA)$
VCO	3.3	45		
FPGA Board	3.3	200		
A-to-D Converter	3.3	1.4		
SPDT Switch	5	1.4		
SP4T Switch	5	160	-5	50

SP16T Switch	5	550	-12	200
IQ Demodulator	5	110	-5	40
Frequency Multiplier	12	102	-5	5
Wideband Amplifier	12	400		
Low Noise Amplifier	12	250		
Power Amplifier	15	900		

As can be seen in Table 11 above, there are some components that require the same input voltage. The VCO, FPGA board, and the A-to-D converter require 3.3V; the SPDT switches requires 5V; the SP16T switch requires a positive supply voltage of 5V and negative supply voltage of -12V; the SP4T switch and the IQ demodulator require 5V and -5V; the frequency multiplier requires 12V and -5V; the wideband amplifier and LNA require supply voltage of 12V; and the power amplifier requires 15V. The power supply can be shared by components that require the same amount of input voltage by placing them parallel to each other on the breadboard. For the components that have positive and negative input voltages, a power supply with differential output for positive, negative, and ground will be used.

2.6 Signal Processing

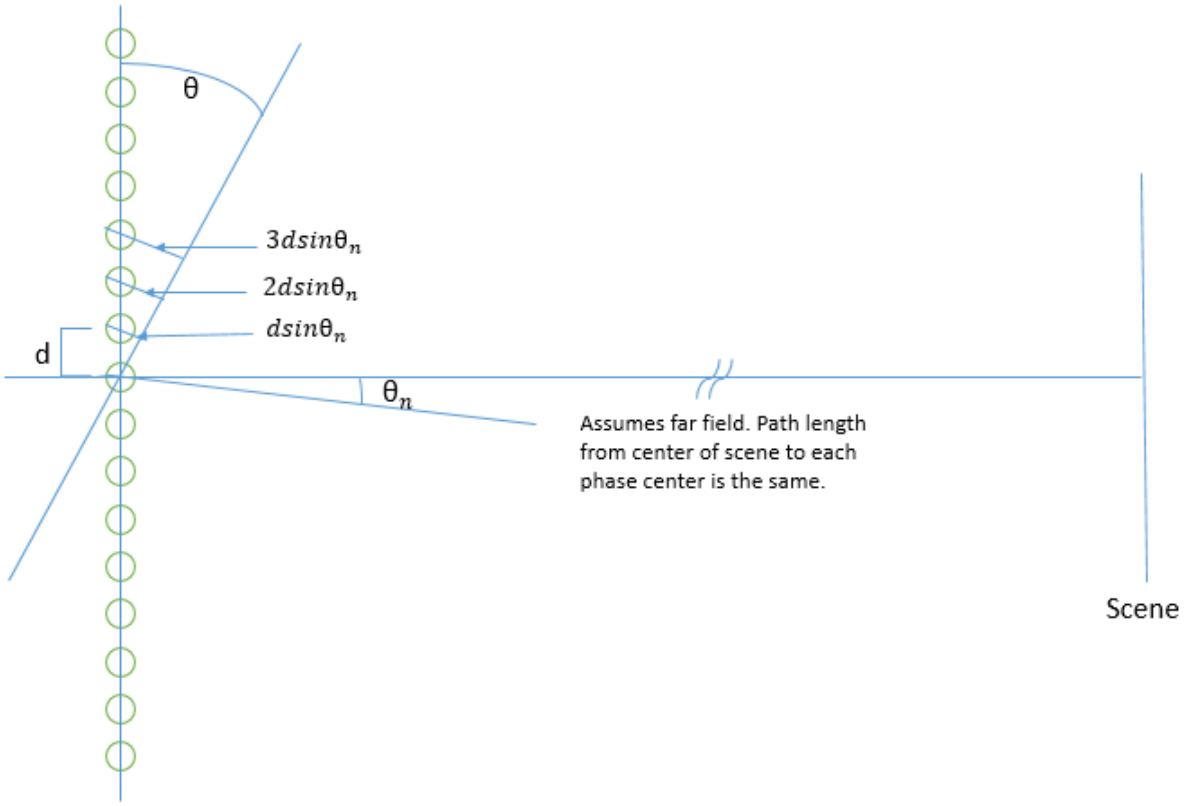

Figure 25. Sixteen Phase Centers from each Tx/Rx Pair to Scene

Figure 25 shows the sixteen phase centers from each transmit and receive antenna pair to the scene. The variable d is the distance between phase centers, θ is the angle from a line with origin at center of array that is 90º to antenna ray to a line from the origin at the center of the array to a point elsewhere in the scene, and θ_n represents the sixteen θs that go to sixteen points in the scene. For each θ, a function with 16 points is generated. The following Table 12 is generated with each of the functions.

Table 12. Sixteen Functions for each Point

	1	2	3	…	15	16
f(θ_1)	1*d*sinθ_1	2*d*sinθ_1	3*d*sinθ_1	…	15*d*sinθ_1	16*d*sinθ_1
f(θ_2)	1*d*sinθ_2	2*d*sinθ_2	3*d*sinθ_2	…	15*d*sinθ_2	16*d*sinθ_2
f(θ_3)	1*d*sinθ_3	2*d*sinθ_3	3*d*sinθ_3	…	15*d*sinθ_3	16*d*sinθ_3
…	1*d*sinθ_n	2*d*sinθ_n	3*d*sinθ_n	…	15*d*sinθ_n	16*d*sinθ_n
f(θ_{15})	1*d*sinθ_{15}	2*d*sinθ_{15}	3*d*sinθ_{15}	…	15*d*sinθ_{15}	16*d*sinθ_{15}
f(θ_{16})	1*d*sinθ_{16}	2*d*sinθ_{16}	3*d*sinθ_{16}	…	15*d*sinθ_{16}	16*d*sinθ_{16}

Each of these functions generates a linear phase slope versus frequency that can be evaluated in Excel. Then each of the functions can be taken and broken into real and imaginary parts. Table 13 is generated with each of the functions for the real part and Table 14 is generated for the imaginary part.

Table 13. Real Part for the Sixteen Functions

	1	2	3	…	15	16
f($real\theta_1$)	cos(d*sinθ_1)	cos(2*d*sinθ_1)	cos(3*d*sinθ_1)	…	cos(15*d*sinθ_1)	cos(16*d*sinθ_1)
f($real\theta_2$)	cos(d*sinθ_2)	cos(2*d*sinθ_2)	cos(3*d*sinθ_2)	…	cos(15*d*sinθ_2)	cos(16*d*sinθ_2)
f($real\theta_3$)	cos(d*sinθ_3)	cos(2*d*sinθ_3)	cos(3*d*sinθ_3)	…	cos(15*d*sinθ_3)	cos(16*d*sinθ_3)
…	cos(d*sinθ_n)	cos(2*d*sinθ_n)	cos(3*d*sinθ_n)	…	cos(15*d*sinθ_n)	cos(16*d*sinθ_n)
f($real\theta_{15}$)	cos(d*sinθ_{15})	cos(2*d*sinθ_{15})	cos(3*d*sinθ_{15})	…	cos(15*d*sinθ_{15})	cos(16*d*sinθ_{15})
f($real\theta_{16}$)	cos(d*sinθ_{16})	cos(2*d*sinθ_{16})	cos(3*d*sinθ_{16})	…	cos(15*d*sinθ_{16})	cos(16*d*sinθ_{16})

Table 14. Imaginary Part for the Sixteen Functions

	1	2	3	…	15	16
f($imag\theta_1$)	sin(d*sinθ_1)	sin(2*d*sinθ_1)	sin(3*d*sinθ_1)	…	sin(15*d*sinθ_1)	sin(16*d*sinθ_1)
f($imag\theta_2$)	sin(d*sinθ_2)	sin(2*d*sinθ_2)	sin(3*d*sinθ_2)	…	sin(15*d*sinθ_2)	sin(16*d*sinθ_2)
f($imag\theta_3$)	sin(d*sinθ_3)	sin(2*d*sinθ_3)	sin(3*d*sinθ_3)	…	sin(15*d*sinθ_3)	sin(16*d*sinθ_3)
…	sin(d*sinθ_n)	sin(2*d*sinθ_n)	sin(3*d*sinθ_n)	…	sin(15*d*sinθ_n)	sin(16*d*sinθ_n)
f($imag\theta_{15}$)	sin(d*sinθ_{15})	sin(2*d*sinθ_{15})	sin(3*d*sinθ_{15})	…	sin(15*d*sinθ_{15})	sin(16*d*sinθ_{15})
f($imag\theta_{16}$)	sin(d*sinθ_{16})	sin(2*d*sinθ_{16})	sin(3*d*sinθ_{16})	…	sin(15*d*sinθ_{16})	sin(16*d*sinθ_{16})

When the real part is graphed, each function plots out as sinusoidal functions of different frequencies, and these are 90° out of phase with the imaginary part. The real and imaginary functions become the basis functions and they will be stored in the VHDL code. They will need to be converted from decimal to fixed point so that they can be operated on.

The hardware provides sixteen I and Q values based on measured data from each of the sixteen phase centers. The IQ demodulator generates sixteen Is at sixteen points, which are the real part, and sixteen Qs at sixteen points, which are the imaginary part, and they are analog voltage values that represent real and imaginary parts of measured return from the scene where the energy is coming in from different angles.

For each angle θ, the image energy at θ can be calculated doing the complex multiply using the following Equation 15:

$$\left[\left(R_{n,\theta\mathrm{n}}\right) - j\left(I_{n,\theta\mathrm{n}}\right)\right] \times \left[\left(I_{nd}\right) + j\left(Q_{nd}\right)\right]$$

Equation 16: Complex Multiply for Basis Function and I and Q Data

This equation can be applied sixteen times for each of the sixteen points with all θs. It can be simplified in the following manner with Equation 17 for the real part and Equation 18 for the imaginary part:

$$f(realcomp\theta_n) = \left(R_{n,\theta 1} \times I_{nd}\right) + \left(I_{n,\theta\mathrm{n}} \times Q_{nd}\right)$$

Equation 17: Complex Multiply for the Real Part

$$f(imagcomp\theta_n) = \left(-I_{n,\theta\mathrm{n}} \times I_{nd}\right) + \left(R_{n,\theta\mathrm{n}} \times Q_{nd}\right)$$

Equation 18: Complex Multiply for the Imaginary Part

In order to get the amplitude for each of the sixteen functions, the real part of each of the sixteen functions for each of the θs will have to be summed and the total sum will be squared, and the same will be done for the imaginary part of each of the sixteen functions for each of the θs. Then these squared values obtained, named $real_{\theta\mathrm{n}}$ and $imag_{\theta\mathrm{n}}$ in this case, will be used to finally calculate the amplitude to be graphed with the following Equation 19:

$$A_n = 20 \times \log\left[\left(real_{\theta\mathrm{n}} + imag_{\theta\mathrm{n}}\right)^{1/2}\right]$$

Equation 19: Amplitude for Each Angle

For image formation, the sum of the energy from some of the scatterers is taken and they are decomposed by multiplying them by the basis functions. The basis function represents the energy that will come in from a different angle, so if it is multiplied by the total energy, it decomposes it into just that part.

With Fourier transform, the amplitude versus time is being calculated; however, in this case, the amplitude versus angle is being calculated. Fourier transform is used to decompose the

waveform into the amounts of energy that come in from different angles. Instead of having a coefficient that represents energy at a frequency, the coefficient of energy that come in at a certain angle is being represented. All of these calculations are part of the long version of the complex Fourier transform at a more physical sense. Appendix A1 shows an example done for the signal processing for further explanation.

3 Schedule

An updated version of the schedule has been provided in Table 15 with the subsequent changes requested by the sponsor. Current tasks that are critical to the completion of this project's schedule include verifying the authorization to use certain vendors for ordering parts, adding new vendors to the university's list of approved vendors and receiving vendor information in return, as well as submitting the final purchase orders for the parts.

The original date to begin ordering parts was scheduled for November 10, 2014. There was a delay in finalizing the components for this antenna design which in turn caused a delay in ordering parts. The delay was caused in part to the Northrop Grumman sponsor approving the team's design and ensuring all necessary parts were included. After a thorough review some parts needed to be removed and new parts added to the list. The one part removed was the D-to-A converter and then several new parts were added to the system including the wideband amplifier, three variable attenuators, and 12 fixed attenuators.

These changes to the components list required additional research to see which models were more suitable for this project as well as contacting vendors to ensure parts were available for immediate order. The new date to begin ordering parts has now been moved to November 18, 2014 pending university approval of select part vendors from Hittite, Fairview Microwave, Minicircuits, Advanced Receivers, RF Lambda, Universal Microwave CMPTS, Digilent, and Marki Microwave. As of now, the deadline to complete the project by April 2015 is not affected by this ordering delay because the parts will not be needed until late January or early February 2015. There is a quick turnaround on part ordering from these vendors, however the main delay is getting the purchase orders approved on the university's behalf.

View Table 15 to see the tentative list of tasks associated with this phase of the project. To see the full Gantt chart reference the appendix section of this report.

Table 15. Tasks List for Milestone #3 to project completion (tentative)

Task Name	Duration	Start	Finish	Resource Names
Prepare Milestone #3 - System-Level Design	**23 days**	**Wed 10/22/14**	**Fri 11/21/14**	
Frequency Justification	**6 days**	**Wed 10/22/14**	**Wed 10/29/14**	**Matthew Cammuse**
Antenna Design Concept	**8 days**	**Wed 10/22/14**	**Fri 10/31/14**	**Matthew**

				Cammuse
Aperture Simulation	8 days	Wed 10/22/14	Fri 10/31/14	Matthew Cammuse
Component Trade-Offs	8 days	Wed 10/22/14	Fri 10/31/14	Matthew Cammuse
Technical Trades	**5 days**	**Mon 10/27/14**	**Fri 10/31/14**	**ALL**
Identify Trades	2 days	Mon 10/27/14	Tue 10/28/14	ALL
Perform Trade-Off Analysis	3 days	Mon 10/27/14	Wed 10/29/14	ALL
Assess Project Risks & Issues	**2 days**	**Mon 10/27/14**	**Tue 10/28/14**	**Jasmine Vanderhorst, Benjamin Mock**
Outline Milestone #3 Report	2 days	Mon 10/27/14	Tue 10/28/14	ALL
Team Meeting - Status Update	**0 days**	**Tue 10/28/14**	**Tue 10/28/14**	**Jasmine Vanderhorst**
FPGA Programming Plan & Concept	**16 days**	**Wed 10/22/14**	**Wed 11/12/14**	**Patrick Delallana**
Signal Processing Code	16 days	Wed 10/22/14	Wed 11/12/14	Julia Kim, Patrick Delallana
Component Trade-offs	6 days	Wed 10/22/14	Wed 10/29/14	Patrick Delallana
Develop Contingency Plan	6 days	Wed 10/22/14	Wed 10/29/14	Patrick Delallana
Analog-To-Digital Converter Code	8 days	Wed 10/29/14	Fri 11/7/14	Patrick Delallana
Discrete Controls	8 days	Wed 10/29/14	Fri 11/7/14	Patrick Delallana
VGA Code	11 days	Wed 10/29/14	Wed 11/12/14	Patrick Delallana
Assess Project Risks & Issues	**2 days**	**Mon 11/3/14**	**Tue 11/4/14**	**Jasmine Vanderhorst, Benjamin Mock**
25% Completion of Milestone 3 Report	5 days	Tue 10/28/14	Mon 11/3/14	ALL
Team Meeting - Status Update	**0 days**	**Tue 11/4/14**	**Tue 11/4/14**	**Jasmine Vanderhorst**
Simulation: Timing/Synchronization	**8 days**	**Wed 10/22/14**	**Fri 10/31/14**	**Patrick Delallana**
Determine Components	5 days	Wed 10/22/14	Tue 10/28/14	Joshua Cushion

Determine Component Timing	3 days	Tue 10/28/14	Thu 10/30/14	Patrick Delallana
Generate Timing Diagram	2 days	Thu 10/30/14	Fri 10/31/14	Patrick Delallana
Finalize Component Budget	3 days	Wed 10/29/14	Fri 10/31/14	Benjamin Mock
Radar Range Equations	**6 days**	**Mon 11/3/14**	**Mon 11/10/14**	**Joshua Cushion**
Signal Calculation	6 days	Mon 11/3/14	Mon 11/10/14	Matthew Cammuse
Noise Calculation	6 days	Mon 11/3/14	Mon 11/10/14	Joshua Cushion
Transmit Path Concept	**6 days**	**Mon 11/3/14**	**Mon 11/10/14**	**Joshua Cushion**
Component Trade-Offs	4 days	Mon 11/3/14	Thu 11/6/14	Joshua Cushion
Perform Analysis	6 days	Mon 11/3/14	Mon 11/10/14	Joshua Cushion
Receive Path Concept	**6 days**	**Mon 11/3/14**	**Mon 11/10/14**	**Joshua Cushion**
Component Trade-Offs	4 days	Mon 11/3/14	Thu 11/6/14	Joshua Cushion
Perform Analysis	6 days	Mon 11/3/14	Mon 11/10/14	Joshua Cushion
Cabling Design Concept	**3 days**	**Thu 11/6/14**	**Mon 11/10/14**	**Patrick Delallana**
Component - Cable Type Selection	3 days	Thu 11/6/14	Mon 11/10/14	Patrick Delallana
Generate Interface Control Document (ICD)	**3 days**	**Mon 11/10/14**	**Wed 11/12/14**	**Patrick Delallana**
"From-To" Diagram - component parameters	3 days	Mon 11/10/14	Wed 11/12/14	Joshua Cushion, Patrick Delallana
Conceptual Mechanical Design	**8 days**	**Mon 11/3/14**	**Wed 11/12/14**	**Malcolm Harmon, Mark Poindexter**
Vendor - Part Ordering	6 days	Mon 11/3/14	Mon 11/10/14	Malcolm Harmon
Mechanical - Part Fabrication/Procure	6 days	Mon 11/3/14	Mon 11/10/14	Mark Poindexter
Material Trade Offs	3 days	Thu 11/6/14	Mon 11/10/14	Mark Poindexter
Material Stress/Strain, Deflection	3 days	Mon 11/10/14	Wed 11/12/14	Malcolm Harmon
Component Layout-Integrated Design	1 day	Wed 11/12/14	Wed 11/12/14	Malcolm Harmon
Assess Project Risks & Issues	2 days	Mon 11/10/14	Tue 11/11/14	Benjamin Mock, Jasmine Vanderhorst

50% Completion of Milestone #3 Report	6 days	Mon 11/3/14	Mon 11/10/14	ALL
Finalize Mechanical Design	**6 days**	**Thu 11/6/14**	**Thu 11/13/14**	**Malcolm Harmon, Mark Poindexter**
Create 2 Trihedral	2 days	Thu 11/6/14	Fri 11/7/14	Mark Poindexter
Create Antenna Frame	3 days	Mon 11/10/14	Wed 11/12/14	Mark Poindexter
Create Frame Wall Mount	3 days	Mon 11/10/14	Wed 11/12/14	Malcolm Harmon
Create Frame Ground Mount	3 days	Mon 11/10/14	Wed 11/12/14	Malcolm Harmon
Create Radar Absorbing Foam Frame	1 day	Wed 11/12/14	Wed 11/12/14	Malcolm Harmon
Detailed Description of Designs	**4 days**	**Mon 11/10/14**	**Thu 11/13/14**	**Mark Poindexter**
Description	3 days	Mon 11/10/14	Wed 11/12/14	Mark Poindexter
Purpose	3 days	Mon 11/10/14	Wed 11/12/14	Mark Poindexter
Trade-Offs	3 days	Tue 11/11/14	Thu 11/13/14	Malcolm Harmon
Power Budget Concept	**6 days**	**Thu 11/6/14**	**Thu 11/13/14**	**Julia Kim**
Voltage Requirements	3 days	Thu 11/6/14	Mon 11/10/14	Julia Kim
Wire and Current Capacity	3 days	Thu 11/6/14	Mon 11/10/14	Julia Kim
PCB Level Shifter	4 days	Mon 11/10/14	Thu 11/13/14	Julia Kim
Testing Concept	**4 days**	**Mon 11/10/14**	**Thu 11/13/14**	**Julia Kim**
Signal Processing Test	4 days	Mon 11/10/14	Thu 11/13/14	Julia Kim, Patrick Delallana
Subassembly Testing Concept	**4 days**	**Mon 11/10/14**	**Thu 11/13/14**	**Julia Kim, Matthew Cammuse**
Transmit Path	2 days	Mon 11/10/14	Tue 11/11/14	Julia Kim, Joshua Cushion
Receive Path	2 days	Mon 11/10/14	Tue 11/11/14	Joshua Cushion, Julia Kim
Full Transmit/Receive Path	2 days	Wed 11/12/14	Thu 11/13/14	Joshua Cushion, Julia Kim
System Calibration Concept	**4 days**	**Mon 11/10/14**	**Thu 11/13/14**	**Julia Kim, Matthew**

				Cammuse
Signal Processing Calibration	4 days	Mon 11/10/14	Thu 11/13/14	Julia Kim
Cabling Calibration - Physical Characteristics	4 days	Mon 11/10/14	Thu 11/13/14	Matthew Cammuse
Team Meeting - Status Update	**0 days**	**Tue 11/11/14**	**Tue 11/11/14**	**Jasmine Vanderhorst**
100% Completion of Milestone #3 Report	5 days	Mon 11/10/14	Fri 11/14/14	ALL
Team Meeting - Presentation Prep	**0 days**	**Tue 11/18/14**	**Tue 11/18/14**	**Jasmine Vanderhorst**
Milestone #3 System-Level Design Final Presentation Due	**0 days**	**Fri 11/21/14**	**Fri 11/21/14**	**ALL**
Procure Storage Facility	**15 days**	**Mon 11/17/14**	**Fri 12/5/14**	**Benjamin Mock**
Verify Vendor Authorization with University	**15 days**	**Mon 11/17/14**	**Fri 12/5/14**	**Benjamin Mock**
Component Ordering (50 parts)	**15 days**	**Tue 11/18/14**	**Mon 12/8/14**	**Benjamin Mock**
FPGA Board (1 unit)	15 days	Tue 11/18/14	Mon 12/8/14	Benjamin Mock
VCO (1 unit)	15 days	Tue 11/18/14	Mon 12/8/14	Benjamin Mock
Power Amplifier (1 unit)	15 days	Tue 11/18/14	Mon 12/8/14	Benjamin Mock
Wideband Amplifier (1 unit)	15 days	Tue 11/18/14	Mon 12/8/14	Benjamin Mock
Antenna Horns (20 units)	15 days	Tue 11/18/14	Mon 12/8/14	Benjamin Mock
Low Noise Amplifier (1 unit)	15 days	Tue 11/18/14	Mon 12/8/14	Benjamin Mock
Frequency Multiplier (2 units)	15 days	Tue 11/18/14	Mon 12/8/14	Benjamin Mock
SPDT Switch (1 unit)	15 days	Tue 11/18/14	Mon 12/8/14	Benjamin Mock
SP4T Switch (1 unit)	15 days	Tue 11/18/14	Mon 12/8/14	Benjamin Mock
SP16T Switch (1 unit)	15 days	Tue 11/18/14	Mon 12/8/14	Benjamin Mock
Variable Attenuator (3 units)	15 days	Tue 11/18/14	Mon 12/8/14	Benjamin Mock
Fixed Attenuators (12 units total)	**15 days**	**Tue 11/18/14**	**Mon 12/8/14**	**Benjamin Mock**
SA18H-07 (3 units)	15 days	Tue 11/18/14	Mon 12/8/14	Benjamin Mock
SA18H-08 (3 units)	15 days	Tue 11/18/14	Mon 12/8/14	Benjamin Mock
SA18H-09 (3 units)	15 days	Tue 11/18/14	Mon 12/8/14	Benjamin Mock
SA18H-10 (3 units)	15 days	Tue 11/18/14	Mon 12/8/14	Benjamin Mock

IQ Demodulator (1 unit)	15 days	Tue 11/18/14	Mon 12/8/14	Benjamin Mock
Analog-To-Digital Converter (2 units)	15 days	Tue 11/18/14	Mon 12/8/14	Benjamin Mock
Band Pass Filter (2 units)	15 days	Tue 11/18/14	Mon 12/8/14	Benjamin Mock
Isolator (1 unit)	15 days	Tue 11/18/14	Mon 12/8/14	Benjamin Mock
Thanksgiving Break	**3 days**	**Thu 11/27/14**	**Sun 11/30/14**	**ALL**
Christmas break	**17 days**	**Mon 12/15/14**	**Tue 1/6/15**	**ALL**
Spring: First Week of Class	**8 days**	**Wed 1/7/15**	**Fri 1/16/15**	**ALL**
System Assembly	**18 days**	**Wed 1/7/15**	**Fri 1/30/15**	**ALL**
Team Meetings - Spring Deliverables & Milestones	6 days	Thu 1/8/15	Thu 1/15/15	ALL
Verify All Components in Secure Storage	5 days	Mon 1/12/15	Fri 1/16/15	ALL
Connect FPGA Board, CPU, and Display	5 days	Mon 1/19/15	Fri 1/23/15	ALL
Construct Electrical Circuit	7 days	Mon 1/19/15	Tue 1/27/15	ALL
Attach Power Supply	3 days	Tue 1/27/15	Thu 1/29/15	ALL
Attach To Structural Supports	2 days	Thu 1/29/15	Fri 1/30/15	ALL
System Testing	**15 days**	**Mon 2/9/15**	**Fri 2/27/15**	**ALL**
Test FPGA Programs	5 days	Mon 2/9/15	Fri 2/13/15	ALL
Test Power Supply	5 days	Mon 2/9/15	Fri 2/13/15	ALL
Test Circuit Components	5 days	Mon 2/9/15	Fri 2/13/15	ALL
Analyze Connectivity	5 days	Mon 2/9/15	Fri 2/13/15	ALL
Record and Analyze Tests	11 days	Fri 2/13/15	Fri 2/27/15	ALL
Result Evaluation	**35 days**	**Mon 3/2/15**	**Fri 4/17/15**	**ALL**
Document Project Progress	5 days	Mon 3/2/15	Fri 3/6/15	ALL
Finalize Project	15 days	Mon 3/9/15	Fri 3/27/15	ALL
Finalize Report	11 days	Sat 3/28/15	Fri 4/10/15	ALL
Present Project Results	5 days	Mon 4/13/15	Fri 4/17/15	ALL
Final Exam Week	**5 days**	**Mon 4/27/15**	**Fri 5/1/15**	**ALL**
End of Year: Graduation	**0 days**	**Sat 5/2/15**	**Sat 5/2/15**	**ALL**

4 Budget Estimate

The operating budget for the SAR Imager team, as provide by Northrop Grumman through the FAMU-Foundation, is set promptly at $50,000. The current expected budget for components is depicted in Table 16.

Table 16

Component	Manufacturer	*Manufacturer Part Number*	*Price ($)*	*Qty.*	*Total Cost*
VCO	*Hittite*	*HMC820LP6CE 1127-2194-ND*	*343*	*2*	*700*
Frequency Multiplier	*Hittite*	*HMC-C056*	*41.95*	*2*	*83.9*
SPDT Switch	*Hittite*	*HMC-C058*	*69.95*	*1*	*69.95*
Power Amplifier	*Fairview Microwave*	*SPA-110-30-01-SMA*	*2,240.27*	*1*	*2240.27*
Low Noise Amplifier	*Fairview Microwave*	*SLNA-120-38-22-SMA*	*1,512.67*	*2*	*3025.34*
Variable Attenuator	*Fairview Microwave*	*SA4077*	*645.38*	*3*	*1936.14*
Fixed Attenuator	*Fairview Microwave*	*SA18H-07*	*49.51*	*3*	*148.53*
Fixed Attenuator	*Fairview Microwave*	*SA18H-08*	*49.5*	*3*	*148.5*
Fixed Attenuator	*Fairview Microwave*	*SA18H-09*	*49.5*	*3*	*148.5*
Fixed Attenuator	*Fairview Microwave*	*SA18H-10*	*49.5*	*3*	*148.5*
Wideband Amplifier	*Mini-Circuits*	*ZVA-183-S+*	*895*	*1*	*895*
Antenna Horns	*Advanced Receiver*	*MA86551*	*20*	*25*	*500*

SP4T	*RF Lambda*	*RFSP4TA0812G*	*1500*	*1*	*1500*
Isolator	*RF Lambda*	*RFLI-501-1*	*125*	*1*	*125*
SP16T Switch	*Universal Microwave*	*UMC SR-L010-16S*	*55*	*1*	*55*
IQ Demodulator	*Polyphase Microwave*	*AD60100B*	*1,225*	*1*	*1225*
Band Pass Filter	*Marki Microwave*	*FB-1050*	*800*	*2*	*1600*
A-D Converter	*Digilent*	*410-064P-KIT*	*40.49*	*2*	*80.98*
FPGA	*Digilent*	*410-182P-KIT*	*189*	*1*	*189*
				Subtotal	*14177.36*

5 Risk Assessment

The construction of the Imager has a critical path as defined in Appendix A3. The following sections outline the potential threats to the successful flow along the critical path and overall project completion. The risks are defined in three strata, Technical Risks, Scheduling Risks, and Budgeting Risks; these sections encompass all potential hazards to the team's ability to reach the expected end product and its deliverables. All risk components will be categorized by their description, probability, consequence, and mitigation strategy.

5.1 Technical Risks

The first stratum encompasses all technical risks associated with facilitating the Imager's design, construction, and testing. These risks stem from the hardware implemented, the role of the antenna horns, and influence of the electrical systems on the mechanical structure and vice versa.

5.1.1 Mechanical Structure Risks

The following subsections define and mitigate the risks associated with the mechanical frame and structural components integration within the Imager's electrical systems. These risks highlight the ability for the team to effectively accomplish their scope deliverables and define the mitigation strategies necessary to overcome said threats.

5.1.1.1 *Structure Risk 1*: Quadrant Stress Increased by Antenna Horns

Description:

Each quadrant of the structure will have 5 antenna horns attached using a pin and bolt to tighten the antenna after it has been correctly aligned. The risk is associated with the arm of each quadrant. The arm will have increasing deflection as each horn is placed on the structure and if the deflection in the arm becomes too great then the horns will lose their alignment. The horn must be vertically and horizontally aligned to receive the optimal response from the signal pulses. Misaligned horns will distort the image generated from the pulse.

Probability: Very Low
Although deflection is a valid risk to be concerned with, the probability of it occurring is very low. The overall weight of the horns placed in the structure will not cause too much deflection. The material chosen, aluminum, for the structure will be sufficiently strong enough to avoid deflection. The objective is to not allow the yield strength of aluminum, 275MPa be overcome by the weight of the horn antennas.

Consequences: Catastrophic
As time passes, if the material chosen does not withstand the weight of the horns, the arm of each quadrant will progressively bend. Ultimately, it could reach its yield point and become deformed to the point where it will lose its elasticity. This will bring the material to eventually fracture. This is catastrophic and will permanently disrupt the signal pulses until the structure is repaired.

Strategy:
Approaches to prevent risk:

1) One way to prevent the effects of over deflection is to be sure the material chosen has been analyzed and calculated to have a yield strength beyond the force of the horns against the arm of the quadrants. This will reduce the amount of deflection in the material and allow the horns to be correctly aligned with one another.

2) Another way to prevent deflection in the quadrants is to properly assembly quadrants with the C-shape brackets. The brackets all custom made to hold the quadrant in a rigid manner to prevent the arm of each quadrant from deflecting. When each quadrant is assembled, the forces acting on it will provide for a more secure yield strength. When each horn is placed into the structure, the forces are equally distributed amongst all of the quadrants.

5.1.1.2 *Structure Risk 2*: Vertical Component Box Increases Power Loss Risk

Description:
Due to the arrangement of the electrical components, the box must be made in an L shape to provide the best electrical flow through all the wires. The reason the box is made into an L shape is because the FPGA Demo Board must be laid horizontally to the bottom surface while the rest of the components are vertically placed into vertical side of the box. Each component must not fall down the component box. This box will be placed on the back of the structure for the convenience of the consumer.

Probability: Very High

Internal flow through the wires already have major loss applied to them. When the wire is bent in any direction, minor losses are formed reducing the current of the wire. This has a very high potential to occur because the design specifies that the FPGA Demo Board will be laid horizontally. The wires from the FPGA to the resulting components must be bent to properly connect the components. This concludes a minor loss in the wires.

Consequences: Moderate
The main consequence of the component box is that the wires will lose current flow due to minor losses. The consequence is minor because the loss in the wires, from appropriate calculations, do not cause a significant difference. To reduce the amount of loss in the wire is vital, but if the L shape box causes bends in the wire, it will still not be enough to effect the remaining components.

Strategy:
The strategy to reduce/prevent loss in the wire is to lay the whole component box flat. To have all the components on a horizontal plane will remove the minor losses formed from the L-shape component box. Although this is an ideal decision to make, to remove the box for the back of the structure and lay flat on a standing stool, the consumer will be at an disadvantage because the structure should be used as a whole.

5.1.1.3 Structure Risk 3: Unaligned Structure Stand can Increase Redirect Signal

Description:
The antenna structure must be held upright for proper use of the antennas. This allows each antenna to be directed to the target with much precision. The structure will be held up by a base stand that can support the weight of the entire structure including the component box. The way the stand is joined to the structure is through a pin and slot joint. A rectangle male end on the stand will be inserted into a female end of the structure. If the joint connection is not perfectly fabricated or wears over time the structure will not properly stand upright and may fall to one side of the stand. The leaning will be caused by the uneven center of gravity on the structure.

Probability: Moderate
The probability of this risk occurring is moderate. With the dimension we chose for the joint and the results produced when Bettinger fabricates the product, there can be error that will cause the joint to not fit as desired. This company has proven its ability to perform to our satisfaction; which is why the probability is at Moderate and no higher.

Consequences: Moderate
The consequences associated with this risk are also moderate. Through calculations of the bore sight for each antenna, it can be noted that even with a slight alignment, the signal pulses have a wide enough range to capture the target as intended. The beam width was calculated to be 25 degrees which is appropriately wide enough to account for error of misalignment in the stand for the structure.

Strategy:
Approaches to prevent risk:

1) The first approach to prevent risk is to be sure all error has been calculated. After calculation, find the appropriate way to reduce the error in the calculation so that the joint connecting the stand to the structure will be rigid enough to hold the antennas in the necessary alignment.
2) If the risk has come to fruition, then a way to repair the problem is to use a seal that will close the gap in the joint. This is called a square cut O-ring that will replace the air gape in the joint and provide a rigid body for the structure-to-stand connection.

5.1.2 Electrical Systems Risks

The following subsections define the risks and threats presented by the challenges that are encompassed under the electrical systems of the imager. The risks analyze the factors that are needed to establish the subsection and illustrate the ability for that step to delay the project schedule. Each subsection provides a clear definition of the mitigation strategies that the team will employ in the event that these risks develop into issues.

5.1.2.1 Component Failure

Description:
The components in the electrical system all have absolute maximum values for characteristics such as input and output voltage, current, power as well as other characteristics. These limits are set by the vendor with the guarantee that the components will operate as they were designed to do so. However if any of these maximums are exceeded the components can become electrically stressed and it is no longer guaranteed that they will operate as they were designed to.

Probability: Low
During the design process the absolute maximum values for each of the characteristics specified were taken into consideration. Good engineering practice was used when designing the electrical system in order to ensure that the maximums were not reached. For example, for components such as the amplifiers and the switches the output power from those components was calculated with enough margins so that P1dB compression points would not be reached.

Consequence: High
If any of the components in the electrical system were to become electrically stressed this could cause the entire electrical system to fail. For example, if the VCO was to become stressed there would be not RF signal generated, or if the SPDT switch was to fail the radar could get stuck in either transmit mode or receive mode.

Strategy:
When designing the electrical system the maximum thresholds were taken into consideration. In order to ensure that they were not exceeded the values used to calculate each characteristic were below the absolute maximums.

5.1.2.2 Software Development Risk

Description:

During the design process, the software design may be inadequate or incomplete as far as the scope of the project is hoped to reach. This includes generating code that will allow the FPGA to generate pulses, control timing of the switches, and if needed the signal processing of the results recorded. This may delay the testing strategies of the project time line and/or completion of the whole project itself.

Probability: Moderate

The coding level required to generate the pulses and timing for the system is not inherently difficult. The only difficulty that may arise will be just figuring out how to match the correct timing with the physical implementation of the project which could include unknown factors. If the PC cannot be used to do image processing using a program like Labview, then the image processing on the FPGA would be another factor that might be difficult to complete. This is because the FPGA used for the system (Digilent Nexys 3) does not come with image processing software.

Consequence: High

If the pulses and timing cannot be generated properly, then it is very hard to show results from the work of this project. This is a vital portion of the project that must be at least partially working to get some results. These results include anywhere from detecting signal with an RF meter, to having imaging on the VGA display.

Strategy:

If the FPGA cannot be programmed in such a way to generate the signals and the timing required for the SAR system, a very simplified version of the system can be utilized by using test equipment. This new system would include a pulse generator to generate the pulse, and a scope to display the image and that would do the image processing. With this new system the FPGA would not be needed. Overall this is just an extreme backup in case nothing else works for this project. If the PC cannot be used to do the Image processing, then the image processing would have to be done on the FPGA.

5.1.2.3 Interface Outside of Scene Extent

Description:

Radiating antennas propagate a main lobe beam with the strongest signal but also weaker grating lobe beams at symmetrical angles directed away from the target. Grating lobe beams need to be absorbed to allow a clean calibration process of the main lobe beam. If the testing room for the radar system is not properly installed with a type of radio frequency absorbing material, calibration of the SAR Imager could be flawed.

Probability: Moderate
After installing radio frequency absorbance material, the worry about excessive grating lobe beams returning a signal should be obsolete. However, the horn antennas being utilized have low gain values, thus the beamwidths cover a large scene extent.

Consequence: Severe
In order to calibrate the radar system, the only radiating beam from the antennas that can create a return signal is the main lobe beam. If grating lobes bounce off of objects away from the scene, the signal processing of the radar system will become slightly or largely flawed.

Strategy:
In order to prevent unnecessary return signals from objects outside of the desired scene extent, radio frequency absorbance materials needs to be installed around the scene extent. A lab room installed with absorbance material would solve the problem of grating lobes interfering with the return signal from the main lobe beam.

5.1.3 Antenna Design Risk

5.1.3.1 *Antenna Design Risk 1*: Phase Center Amount

Description:
The overall antenna design is meant create 16 phase centers per linear antenna array. If the spacing between the phase centers is not relatively precise, the amount of phase centers could fail to equal 32 overall.

Probability: Low
Properly spacing the antennas should not be a challenging task. Multiple tests, using laser pointers and other measuring tools, can reassure the distances between each antenna and theoretically the right amount of phase centers should be create.

Consequences: Severe
If 16 phase centers are not properly created per antenna array, the signal processing calculations could become erroneous. The location where the receive signal generated from could be inaccurate.

Strategy:
Checking the alignment of the antennas will have be a priority to confirm the creation of 16 phase centers. Alignment tools like laser points and measuring apparatus will have to be utilized.

5.1.4 Signal Processing Risks

5.1.4.1 *Signal Processing Risks 1*: I-data and Q-data Not Collected

Description:
There is a risk that the data from the I-channel and the Q-channel are not collected from the IQ demodulator and stored in the FPGA board.

Probability: Low
The probability that the data is not collected properly is low as the FPGA board will be programmed to receive the information.

Consequences: Minor
There is an alternate way to get the data without having to rely solely on the programming, so the consequences are not significant.

Strategy:
A voltmeter can be attached to the I-channel and the Q-channel of the demodulator to get the data manually. This measured data will then be entered into an Excel spreadsheet that is set up as a backup, which will then be used to calculate the 16 amplitudes for image formation.

5.2 Schedule Risks

The following section depicts how the Gantt Chart's functions affect the successfully completion of the project deliverables. This section focuses on the potential complications as they relate to the critical path (refer to Appendix A3). Each section will note the necessary mitigation strategies and define all consequences of schedule.

5.2.1 Component Ordering

The following subsection illustrates the various areas involved within the component procurement process and highlights the points at which the project plan can deviate from expected.

5.2.1.1 Vendor Approval/Registration

Description:
Accessing funds through the FAMU Foundation requires that a purchase order must be placed with an approved vendor in order to procure the necessary components. Most of the vendors listed in the budget assessment are not currently registered vendors with FAMU, this amounts to additional lead time when acquiring components. The risks associated with this include a vendor not being able to be registers, by either not supplying a W-9 form and accepting purchase orders; or extending the delivery time and by extension extending the time to begin testing.

Probability: Low
The team has contacted the vendors listed in the budget assessment and they are willing to supply W-9 forms and accept purchase orders. The only reason that the vendors would not be

registered would be by denial by FAMU, which has been established as a low probability of occurrence.

Consequence: Severe
Should a vendor be prevented from registering with FAMU the team will need to select a secondary vendor and place a separate purchasing order. This consequence was labeled as severe in that purchase orders are only placed for orders that exceed $100; as this may place the team in a situation where they would have to front the money for the part, or extraneous parts would need to be ordered to allow use of purchase ordering. Additionally, should a vendor fail to register with FAMU, the team will have to readjust their testing plan if a part lies along the critical path or the secondary option does not flow with the testing plan currently in place.

Strategy:
The team has placed the necessary information with Donna Butka for ordering so that enough time exists should a replacement vendor need be contacted. The team also in place alternative components, where possible, should the situation arise.

5.2.1.2 Purchase Order & Delivery Lead Time

Description:
The time of delivery of an ordered component is increased by the need to place and process a purchase order through the Department of Electrical Engineering with Donna Butka. This process has an average extension of delivery by 5 business days. This fluid time extension may increase the delivery time beyond what has been planned for extending the waiting time before testing can occur.

Probability: Moderate
The probability for this occurrence was established at moderate with an understanding that the university will be open for only for a few more weeks before the winter break, this may cause an increase in the amount of business days it takes to process requests for a purchase order.

Consequence: Moderate
The consequence for an unanticipated lead time is rather moderate, as the team developed time into the project time line for many components to be ordered in late November. This time frame will allow for an additional five business days to be added unexpectedly.

Strategy:
The team has planned the testing strategy in the project time line behind the longest delivery time (FPGA) so that additional time could be accounted for should the additional business days be required to process the purchasing requests.

5.2.1.3 Storage Facility

Description:
The delivered components and subassemblies will need to be stored in a secure location large enough to hold the mechanical frame and all of the electrical components, as they arrive. Space within the College of Engineering and other facilities around Innovation Park is especially

limited, acquiring an available storage proves to be a challenging aspect to the completion of this product.

Probability: High
There has yet been an available space for the team to store their components and finding such a space has proven rather difficult. The probability was set as high to indicate the necessity and the difficulty in finding a secure location to store all of this equipment at the appropriate testing environment.

Consequence: Severe
Not having a secure and singular location to store all of the test equipment will have severe consequences, such as having multiple storage locations across Innovation Park which may result in the loss of parts and unequal storage conditions that may alter the performance of electrical components. In the event that a secure location is not able to be found, the team has not defined a plan that is most suitable for containing these components.

Strategy:
The team plans to contact the EE/ECE, ME, and IE departments if there is storage within the College of Engineering. The team will also contact the High Performance Materials Institute (HPMI), the Aero-Propulsion, Mechatronics, and Energy Building (AME), and the Center for Advanced Power Systems (CAPS) to determine if there is available storage. In the event that these facilities are not available, the team will contact other centers and institutes throughout Innovation Park.

5.2.1.4 Testing Facility

Description:
The need for an appropriate testing facility at the necessary environment presents another challenge. The antenna horns' production of side lobes demand the use of RADAR absorbing foam to prevent the detection of metal from outside the scene extent and the 20 antenna horns require nearly an entire room to be covered in such foam. Additionally, the 20' range of the radar requires that the testing facility also be able to accommodate enough space for at least 8 users for testing. The size of the necessary testing facility presents another challenge when determining the most appropriate facility for testing.

Probability: Moderate
The probability of finding an appropriate facility for testing is moderate for the reason that the EE/ECE department has offered to allow to test in their old portable, which is an all metal container. This may not be the most optimal, but it is a failsafe should other facilities not be able to accommodate our demands.

Consequence: Severe
Without the appropriate facility to test in then the Imager cannot be tested for its effectiveness as defined in the project scope.

Strategy:

The team has contacted the FSU Physics Department about using their Faraday Cage room, and they have contacted HPMI, CAPS, and AME as well to ask about testing availability. The fail safe will be utilizing the portable as described above.

5.3 Budget Risks

The following section illustrates the threats to the completion of the project as they relate to the $50,000.00 budget and the methods used to access these funds. The risks will be defined and expressed in means of probability and then will be mitigated by a strategy the team has put into place.

5.3.1 Purchase Order Minimum

Description:
The minimum amount needed to be spent before a purchase order can be placed is $100.00. On components that are valued less than this amount, the design team is expected to front the expense to these components and then be reimbursed by the FAMU Foundation. The stipulation of refunds is that the FAMU Foundation will only reimburse FAMU students, leaving the entire obligation in the hands of only one student.

Probability: High
There are a large number of components that are required that cost less than $100.00, so the chance that the funds will need to be fronted is significant.

Consequence: Severe
Readjusting the order scheduling around the available funds of one student may prevent many components from being ordered in the time allotted and could harm the completion of the project. This event has severe consequences because the already tight schedule can not afford to be extended beyond what it has already been allotted.

Strategy:
The team plans to order all components from one vendor in one order to ensure that the minimum $100.00 is reached with every order. The team also plans to order multiple components where necessary to ensure the a purchase order may be used.

5.4 Summary of Risk Status

The risk to the completion of the project schedule exists moderately and the team has defined clear strategies to mitigating all risks, especially as they pertain to the critical path. In the event that a risk gives rise to an issue the developed strategies appear sufficient for the team to effectively overcome any challenge that may occur.

6 Conclusion

Developing an SAR Imager is a challenging project with ambitious goals, but the developmental process has been continuing at a steady pace. The first set of theoretical simulations and design values and schematics are complete. The antenna design is nearly finalized with the necessary design dimensions and horn antennas types being selected. Finalizing the antenna structure, which will hold the overall antenna aperture, is nearly finalized but waiting on the final selection of components so the mechanical engineers can confirm wait distribution. For the components, noise figure and system temperature analysis has been under detailed scrutiny. Helpful excel tables have allowed for easy analysis of components when comparing different types of components or adding and removing components when editing the overall component configuration. After a few more virtual tests and confirmations for Northup Grumman's advisor, Pete Stenger, the components and antennas for the SAR Imager will be finalized and ordered.

The software contribution to the design, which is the more challenging part of the project, has also made major strides. For the FPGA, theoretical approaches have been constructed to how to the FPGA needs to be utilized for the radar system. A timing diagram and procedural block diagrams have been assembled to make the actual programming installment of the radar system easier to understand and demonstrate how the FPGA needs to communicate to multiple components. The FPGA has been ordered and once received, programming the FPGA can begin. The signal processing software is in the creation process with a few early simulations already constructed. Having data analysis at near-real time, the signal processing will be easier. However, the most challenging part of the software design for the radar system will be storing the information outputted by the demodulator.

With the help of the project's advisor, Mr. Stenger, completion of a prototype seems plausible. With each new major milestone of the project, Mr. Stenger has been able to discuss and teach the design group about new concepts about radar, allowing the group to continue working at steady momentum. The design group is confident that a limited prototype can be finalized and constructed for testing.

Reference

[1] CenterPoint Energy, "Humidity & the Indoor Environment," 2006. [Online]. Available: http://www.centerpointenergy.com/staticfiles/CNP/Common/SiteAssets/doc/Humidity_indoor_environ%5B1%5D.pdf. [Accessed 13 October 2014].

[2] Digilent, [Online]. Available: http://www.digilentinc.com/Products/Detail.cfm?NavTop=2&NavSub=451&Prod=NEXYS2&CFID=6418481&CFTOKEN=ed68fb48cc4c26fa-AF6E6B08-5056-0201-02D88BCB17A8A8EC. [Accessed 14 09 2014].

[3] Digilent, [Online]. Available: http://www.digilentinc.com/Products/Detail.cfm?NavPath=2,400,897&Prod=NEXYS3&CFID=6418481&CFTOKEN=ed68fb48cc4c26fa-AF6E6B08-5056-0201-02D88BCB17A8A8EC. [Accessed 09 10 2014].

[4] Digilent, [Online]. Available: http://www.digilentinc.com/Products/Detail.cfm?NavTop=2&NavSub=451&Prod=NEXYS2&CFID=6418481&CFTOKEN=ed68fb48cc4c26fa-AF6E6B08-5056-0201-02D88BCB17A8A8EC. [Accessed 09 10 2014].

[5] Digilent, "Digilent PmodAD1 Digital to Analog Module Converter Board Reference Manual," 2005. [Online]. Available: http://www.digilentinc.com/Data/Products/PMOD-DA1/Pmod%20DA1_rm.pdf. [Accessed 20 October 2014].

[6] Digilent, "Digilent PmodAD1 Analog to Digital Model Converter Board Reference Manual," 2011. [Online]. Available: http://www.digilentinc.com/Data/Products/PMOD-AD1/Pmod%20AD1_rm.pdf. [Accessed 20 October 2014].

[7] Hittite Microwave Corporation, "Electronic Components Datasheet," 2014. [Online]. Available: http://pdf1.alldatasheet.com/datasheet-pdf/view/243103/HITTITE/HMC-C028.html. [Accessed 20 October 2014].

[8] RF Microwave Devices, "High Reliability Military and Space VCO," 2014. [Online]. Available: http://www.bdtic.com/DataSheet/RFMD/VCO-520S.pdf. [Accessed 20 October 2014].

[9] Polyphase Microwave, "Quadrature Demodulator," 2011. [Online]. Available: http://www.polyphasemicrowave.com/datasheets/AD60100B.pdf. [Accessed 20 October 2014].

[10] Hittite Microwave Corporation, "GaAs MMIC SPDT NON-REFLECTIVE," [Online]. Available: http://www.hittite.com/content/documents/data_sheet/hmc-c058.pdf. [Accessed 20 October 2014].

[11] MathWorks, "HDL Coder," 2014. [Online]. Available: http://www.mathworks.com/products/hdl-coder/features.html. [Accessed 20 October

2014].

[12] National Instruments, "LabVIEW FPGA Module," 2014. [Online]. Available: http://www.ni.com/labview/fpga/. [Accessed 20 October 2014].

[13] Mini-Circuits, "The Prevention and Control of Electrostatic Discharge (ESD)," 20 August 2003. [Online]. Available: http://www.minicircuits.com/app/AN40-005.pdf. [Accessed 16 October 2014].

[14] CNN Library, "CNN," Cable News Network, 13 July 2014. [Online]. Available: http://www.cnn.com/2013/07/19/us/colorado-theater-shooting-fast-facts/. [Accessed 12 October 2014].

[15] C. L. Ray Sanchez, "CNN," Cable Network News, 29 December 2013. [Online]. Available: http://www.cnn.com/2013/12/27/justice/connecticut-newtown-shooting-report/. [Accessed 12 October 2014].

[16] H. Martin, "Controversial full-body scanners to be removed from airports," Los Angeles Times - Business, 18 January 2013. [Online]. Available: http://articles.latimes.com/2013/jan/18/business/la-fi-tsa-rapiscan-20130119. [Accessed 12 October 2014].

[17] United States Department of Labor, "Occupational Employment and Wages, May 2013," Bureau of Labor Statistics, 1 April 2014. [Online]. Available: http://www.bls.gov/OES/current/oes172071.htm#%283%29. [Accessed 12 October 2014].

[18] United States Department of Labor, "Occupational Employment and Wages, May 2013," Bureau of Labor Statistics, 1 April 2014. [Online]. Available: http://www.bls.gov/OES/current/oes172141.htm. [Accessed 12 October 2014].

[19] United States Department of Labor, "Occupational Employment and Wages, May 2013," Bureau of Labor Statistics, 1 April 2014. [Online]. Available: http://www.bls.gov/OES/current/oes172112.htm. [Accessed 12 October 2014].

[20] United States Department of Labor, "Occupational Employment and Wages, May 2013," Bureau of Labor Statistics, 1 April 2014. [Online]. Available: http://www.bls.gov/OES/current/oes113051.htm. [Accessed 1 October 2014].

[21] United State Department of Energy, "Office of Management," [Online]. Available: http://professionals.pr.doe.gov/srs/pdf/laborrates_fringe.pdf. [Accessed 12 October 2014].

Appendix

A1 Signal Processing Example

In the following example for signal processing, the start value for θ is -8° and the end value is 8°, and in order to make it symmetrical for sixteen points, an increment of 1.0667 was found. The following Table 17 shows each value for angle θ, both in degrees and radians.

Table 17. Values for the Sixteen Angles

	Degrees	**Radians**
θ_1	-8	-0.13963
θ_2	-6.93333	-0.12101
θ_3	-5.86667	-0.10239
θ_4	-4.8	-0.08378
θ_5	-3.73333	-0.06516
θ_6	-2.66667	-0.04654
θ_7	-1.6	-0.02793
θ_8	-0.53333	-0.00931
θ_9	0.533333	0.009308
θ_{10}	1.6	0.027925
θ_{11}	2.666667	0.046542
θ_{12}	3.733333	0.065159
θ_{13}	4.8	0.083776
θ_{14}	5.866667	0.102393
θ_{15}	6.933333	0.121009
θ_{16}	8	0.139626

The spacing between phase centers in radians was found to be $d = 6\pi \approx 18.85$. By replacing these values into the equations, the following Table 18 for the basis functions can be found.

Table 18. Basis Functions for the Sixteen Angles

	1*d*sin(θn)	**2*d*sin(θn)**	**3*d*sin(θn)**	**4*d*sin(θn)**	**…**	**16*d*sin(θn)**
f(θ1)	-2.623351149	-5.246702299	-7.870053448	-10.4934046	…	-41.97361839
f(θ2)	-2.27541248	-4.550824961	-6.826237441	-9.101649922	…	-36.40659969
f(θ3)	-1.926685206	-3.853370412	-5.780055619	-7.706740825	…	-30.8269633
f(θ4)	-1.577290187	-3.154580375	-4.731870562	-6.309160749	…	-25.236643
f(θ5)	-1.227348516	-2.454697032	-3.682045548	-4.909394064	…	-19.63757626
f(θ6)	-0.876981474	-1.753962948	-2.630944422	-3.507925896	…	-14.03170358
f(θ7)	-0.526310491	-1.052620981	-1.578931472	-2.105241962	…	-8.420967849
f(θ8)	-0.1754571	-0.3509142	-0.5263713	-0.7018284	…	-2.8073136

f(θ9)	0.1754571	0.3509142	0.5263713	0.7018284	…	2.8073136
f(θ10)	0.526310491	1.052620981	1.578931472	2.105241962	…	8.420967849
f(θ11)	0.876981474	1.753962948	2.630944422	3.507925896	…	14.03170358
f(θ12)	1.227348516	2.454697032	3.682045548	4.909394064	…	19.63757626
f(θ13)	1.577290187	3.154580375	4.731870562	6.309160749	…	25.236643
f(θ14)	1.926685206	3.853370412	5.780055619	7.706740825	…	30.8269633
f(θ15)	2.27541248	4.550824961	6.826237441	9.101649922	…	36.40659969
f(θ16)	2.623351149	5.246702299	7.870053448	10.4934046	…	41.97361839

In Figure 26, it can be seen how each of these functions for each angle θ is linear with different slopes.

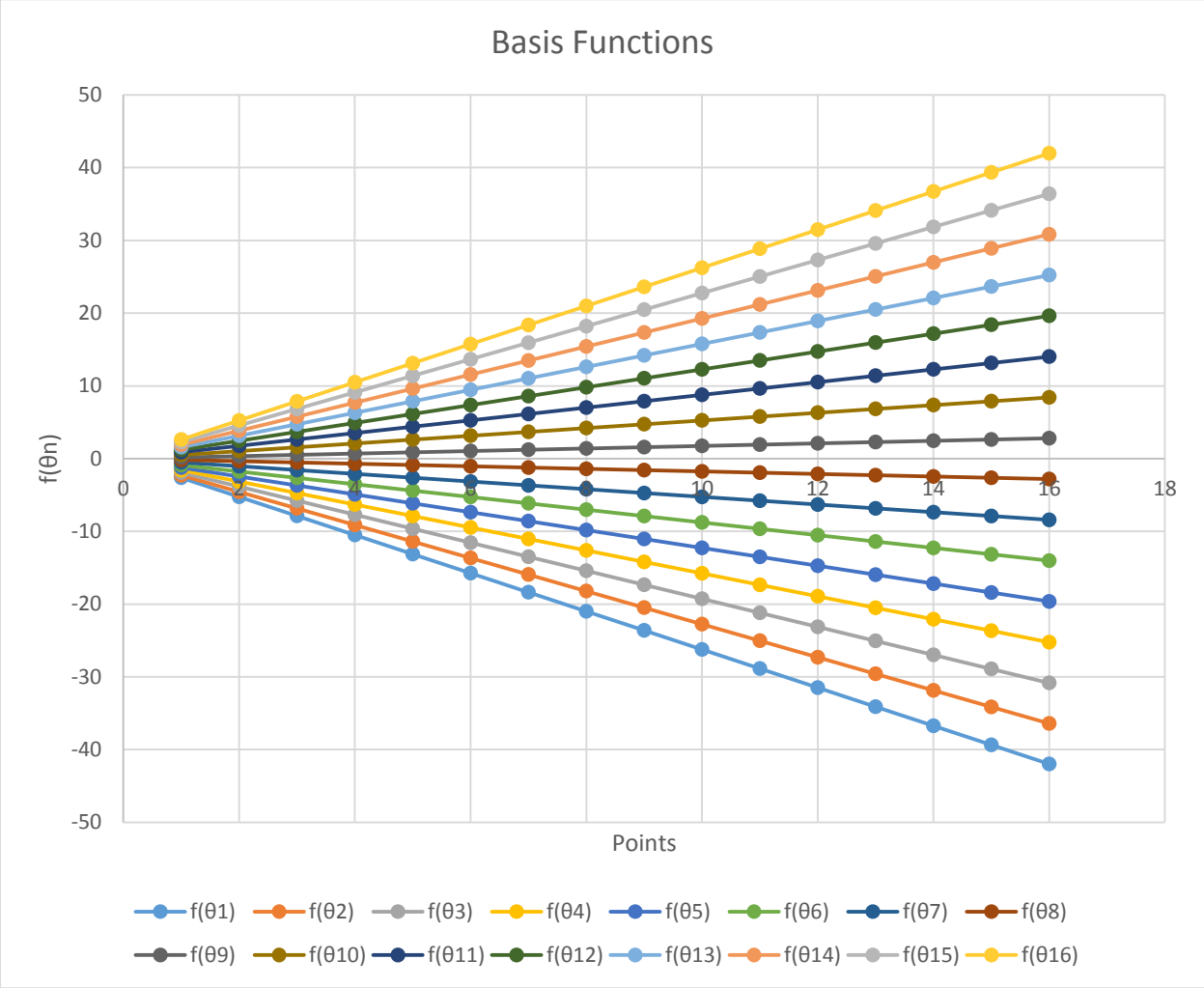

Figure 26. Linear Phase Slope for each function

Each of the functions are then broken into real and imaginary parts. The real part of the basis functions is shown in Table 19, while the imaginary part is shown in Table 20.

Table 19. Real Part of Basis Functions

	cos(1*d*sin(θn))	**cos(2*d*sin(θn))**	**cos(3*d*sin(θn))**	**cos(4*d*sin(θn))**	**…**	**cos(16*d*sin(θn))**
f(realθ_1)	-0.868691599	0.509250189	-0.016071122	-0.481328491	…	-0.42402264
f(realθ_2)	-0.64774144	-0.160862054	0.856135477	-0.948246799	…	0.274706236
f(realθ_3)	-0.348423682	-0.757201875	0.876077814	0.146709359	…	0.831517047
f(realθ_4)	-0.006493815	-0.999915661	0.019480349	0.999662657	…	0.994607066
f(realθ_5)	0.336735543	-0.773218348	-0.857475744	0.195733227	…	0.705250197
f(realθ_6)	0.639474733	-0.182144131	-0.872427872	-0.933647031	…	0.105267962
f(realθ_7)	0.864666364	0.495295842	-0.008135055	-0.509364059	…	-0.537092293
f(realθ_8)	0.984646851	0.939058843	0.864635815	0.763663022	…	-0.944647089
f(realθ_9)	0.984646851	0.939058843	0.864635815	0.763663022	…	-0.944647089
f(realθ_{10})	0.864666364	0.495295842	-0.008135055	-0.509364059	…	-0.537092293
f(realθ_{11})	0.639474733	-0.182144131	-0.872427872	-0.933647031	…	0.105267962
f(realθ_{12})	0.336735543	-0.773218348	-0.857475744	0.195733227	…	0.705250197
f(realθ_{13})	-0.006493815	-0.999915661	0.019480349	0.999662657	…	0.994607066
f(realθ_{14})	-0.348423682	-0.757201875	0.876077814	0.146709359	…	0.831517047
f(realθ_{15})	-0.64774144	-0.160862054	0.856135477	-0.948246799	…	0.274706236
f(realθ_{16})	-0.868691599	0.509250189	-0.016071122	-0.481328491	…	-0.42402264

Table 20. Imaginary Part of Basis Functions

	sin(1*d*sin(θn))	**sin(2*d*sin(θn))**	**sin(3*d*sin(θn))**	**sin(4*d*sin(θn))**	**…**	**sin(16*d*sin(θn))**
f(imagθ_1)	-0.495353314	0.860618525	-0.999870851	0.876540292	…	0.905651589
f(imagθ_2)	-0.761860241	0.986976899	-0.516751435	-0.317534262	…	0.961528202
f(imagθ_3)	-0.937337153	0.653180925	0.482169746	-0.989179642	…	0.555499235
f(imagθ_4)	-0.999978915	0.012987356	0.99981024	-0.025972521	…	-0.103714922
f(imagθ_5)	-0.941599264	-0.634139879	0.51452439	0.98065718	…	-0.708958503
f(imagθ_6)	-0.768812113	-0.983271842	-0.488742885	0.35819439	…	-0.994443893
f(imagθ_7)	-0.502346573	-0.868724369	-0.99996691	-0.860551135	…	-0.843523484
f(imagθ_8)	-0.174558238	-0.343756439	-0.502399152	-0.645615047	…	-0.328088216
f(imagθ_9)	0.174558238	0.343756439	0.502399152	0.645615047	…	0.328088216
f(imagθ_{10})	0.502346573	0.868724369	0.99996691	0.860551135	…	0.843523484
f(imagθ_{11})	0.768812113	0.983271842	0.488742885	-0.35819439	…	0.994443893
f(imagθ_{12})	0.941599264	0.634139879	-0.51452439	-0.98065718	…	0.708958503
f(imagθ_{13})	0.999978915	-0.012987356	-0.99981024	0.025972521	…	0.103714922
f(imagθ_{14})	0.937337153	-0.653180925	-0.482169746	0.989179642	…	-0.555499235
f(imagθ_{15})	0.761860241	-0.986976899	0.516751435	0.317534262	…	-0.961528202

f(imagθ_{16})	0.495353314	-0.860618525	0.999870851	-0.876540292	…	-0.905651589

In Figure 27 shown below, each row for the sixteen points for each of the sixteen real parts of the basis functions have been plotted out and graphed, and in Figure 28, each row the sixteen points for each of the sixteen imaginary parts of the basis functions have been plotted out and graphed. As can be seen, they are both sinusoidal functions of different frequencies, and the imaginary part is 90° out of phase with the real part.

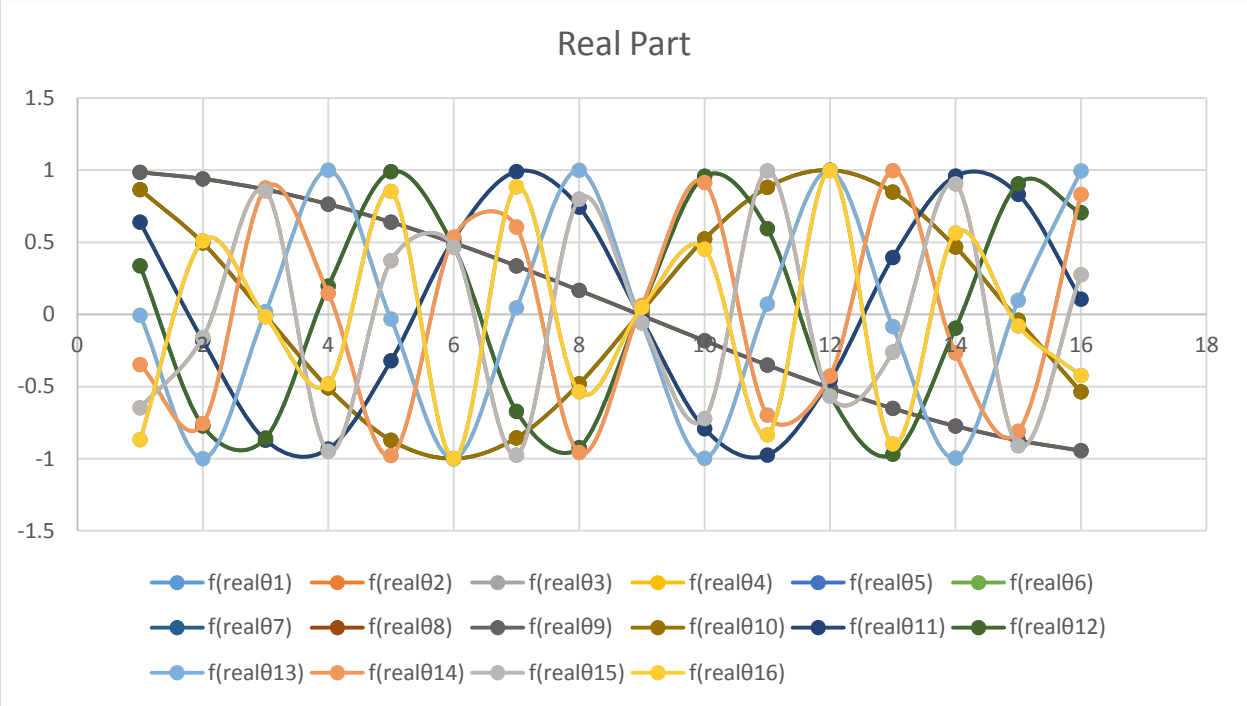

Figure 27. Real Part of the Basis Functions

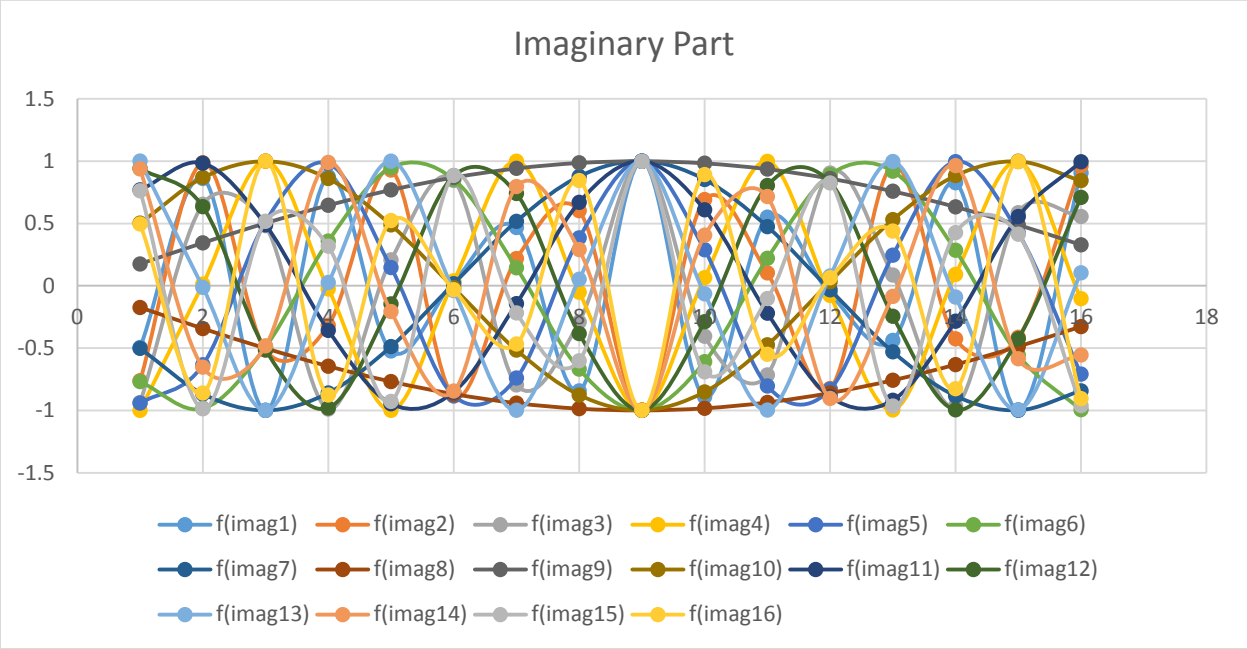

Figure 28. Imaginary Part of Basis Functions

For this example, there is energy coming in from angles θ_4, θ_6, θ_8, θ_{11}, and θ_{14}, so the data from the demodulator would reflect this information. The I data would be the sum of the real part of the basis functions for those angles, which would be the sum of each of the sixteen points of f(realθ_4), f(realθ_6), f(realθ_8), f(realθ_{11}), and f(realθ_{14}), while the Q data would be the sum of the imaginary part of the basis functions for those angles. Each column of Table 21 shows the I data that sums each of the points for the real part at the specified angles for the corresponding column, while each column Table 22 shows the Q data that sums each of the points for the imaginary part at the specified angles for the corresponding column. For example, for column 1 in Table 21 below, it shows the following sum for f(Iθ_1) through f(Iθ_{16}):

$$f(I\theta_{n,1}) = (\cos(1 * d * \sin(\theta_4))) + (\cos(1 * d * \sin(\theta_6))) + (\cos(1 * d * \sin(\theta_8))) + (\cos(1 * d * \sin(\theta_{11}))) + (\cos(1 * d * \sin(\theta_{14})))$$

$$f(I\theta_{n,1}) = (-0.006493815) + (0.639474733) + (0.984646851) + (0.639474733) + (-0.348423682) = 1.908679$$

The same is done for column 1 in Table 22 below, which shows the following sum for f(Qθ_1) through f(Qθ_{16}), except with the imaginary part:

$$f(Q\theta_{n,1}) = (\sin(1 * d * \sin(\theta_4))) + (\sin(1 * d * \sin(\theta_6))) + (\sin(1 * d * \sin(\theta_8))) + (\sin(1 * d * \sin(\theta_{11}))) + (\sin(1 * d * \sin(\theta_{14})))$$

$$f(Q\theta_{n,1}) = (-0.999978915) + (-0.768812113) + (-0.174558238) + (0.768812113) + (0.937337153) = -0.2372$$

Table 21. I data with Energy from θ_4, θ_6, θ_8, θ_{11}, and θ_{14}

	1	**2**	**3**	**4**	**…**	**16**
f(Iθ$_1$)	1.908679	-1.18235	0.015338	0.042741	…	1.092013
f(Iθ$_2$)	1.908679	-1.18235	0.015338	0.042741	…	1.092013
f(Iθ$_3$)	1.908679	-1.18235	0.015338	0.042741	…	1.092013
f(Iθ$_4$)	1.908679	-1.18235	0.015338	0.042741	…	1.092013
f(Iθ$_5$)	1.908679	-1.18235	0.015338	0.042741	…	1.092013
f(Iθ$_6$)	1.908679	-1.18235	0.015338	0.042741	…	1.092013
f(Iθ$_7$)	1.908679	-1.18235	0.015338	0.042741	…	1.092013
f(Iθ$_8$)	1.908679	-1.18235	0.015338	0.042741	…	1.092013
f(Iθ$_9$)	1.908679	-1.18235	0.015338	0.042741	…	1.092013
f(Iθ$_{10}$)	1.908679	-1.18235	0.015338	0.042741	…	1.092013
f(Iθ$_{11}$)	1.908679	-1.18235	0.015338	0.042741	…	1.092013
f(Iθ$_{12}$)	1.908679	-1.18235	0.015338	0.042741	…	1.092013
f(Iθ$_{13}$)	1.908679	-1.18235	0.015338	0.042741	…	1.092013
f(Iθ$_{14}$)	1.908679	-1.18235	0.015338	0.042741	…	1.092013
f(Iθ$_{15}$)	1.908679	-1.18235	0.015338	0.042741	…	1.092013
f(Iθ$_{16}$)	1.908679	-1.18235	0.015338	0.042741	…	1.092013

Table 22. Q data with Energy from θ_4, θ_6, θ_8, θ_{11}, and θ_{14}

	1	**2**	**3**	**4**	**…**	**16**
f(Qθ$_1$)	-0.2372	-0.98395	0.015241	0.317592	…	-0.9873
f(Qθ$_2$)	-0.2372	-0.98395	0.015241	0.317592	…	-0.9873
f(Qθ$_3$)	-0.2372	-0.98395	0.015241	0.317592	…	-0.9873
f(Qθ$_4$)	-0.2372	-0.98395	0.015241	0.317592	…	-0.9873
f(Qθ$_5$)	-0.2372	-0.98395	0.015241	0.317592	…	-0.9873
f(Qθ$_6$)	-0.2372	-0.98395	0.015241	0.317592	…	-0.9873
f(Qθ$_7$)	-0.2372	-0.98395	0.015241	0.317592	…	-0.9873
f(Qθ$_8$)	-0.2372	-0.98395	0.015241	0.317592	…	-0.9873
f(Qθ$_9$)	-0.2372	-0.98395	0.015241	0.317592	…	-0.9873
f(Qθ$_{10}$)	-0.2372	-0.98395	0.015241	0.317592	…	-0.9873
f(Qθ$_{11}$)	-0.2372	-0.98395	0.015241	0.317592	…	-0.9873
f(Qθ$_{12}$)	-0.2372	-0.98395	0.015241	0.317592	…	-0.9873
f(Qθ$_{13}$)	-0.2372	-0.98395	0.015241	0.317592	…	-0.9873
f(Qθ$_{14}$)	-0.2372	-0.98395	0.015241	0.317592	…	-0.9873
f(Qθ$_{15}$)	-0.2372	-0.98395	0.015241	0.317592	…	-0.9873
f(Qθ$_{16}$)	-0.2372	-0.98395	0.015241	0.317592	…	-0.9873

Now that there is data for the I channel and the Q channel at the angles specified, they will be used to perform a complex multiplication for each of the points for the sixteen angles. Table 23 shows the results of the complex multiply realized for each point for the real part. For example, for point 1 of f(realcompθ_1), which is the complex multiply for the real part of θ_1, the following was performed:

$$f(realcomp\theta_{1,1}) = (R_{1,\theta1} \times I_{1d}) + (I_{1,\theta1} \times Q_{1d})$$

$$f(realcomp\theta_{1,1}) = [f(real\theta_{1,1}) \times f(I\theta_{1,1})] + [f(imag\theta_{1,1}) \times f(Q\theta_{1,1})]$$

$$f(realcomp\theta_{1,1}) = [(-0.868691599)(1.908679)] + [(-0.495353314)(-0.2372)]$$
$$= -1.54055545$$

Table 23. Real Part after Complex Multiply

	1	**2**	**3**	**4**	**…**	**16**
f(realcompθ_1)	-1.54055545	-1.448916014	-0.015485876	0.2578098	…	-1.357190177
f(realcompθ_2)	-1.055617118	-0.780941168	0.00525562	-0.141375358	…	-0.649336309
f(realcompθ_3)	-0.44269253	0.252577955	0.0207864	-0.307885113	…	0.359581669
f(realcompθ_4)	0.224800392	1.169468327	0.015537244	0.034477891	…	1.188521783
f(realcompθ_5)	0.866067345	1.538174298	-0.00531012	0.319814777	…	1.47009876
f(realcompθ_6)	1.402914113	1.182847895	-0.020830599	0.073854714	…	1.096770793
f(realcompθ_7)	1.769526983	0.269169819	-0.015365615	-0.295074937	…	0.246301
f(realcompθ_8)	1.920779805	-0.772054213	0.005604748	-0.172402519	…	-0.707644579
f(realcompθ_9)	1.837969376	-1.448532514	0.020919223	0.237681925	…	-1.355489126
f(realcompθ_{10})	1.531213768	-1.440392879	0.01511606	0.251533503	…	-1.419324476
f(realcompθ_{11})	1.038189646	-0.752132778	-0.005932404	-0.153664685	…	-0.866862838
f(realcompθ_{12})	0.419372654	0.29025042	-0.020994205	-0.303083118	…	0.070185935
f(realcompθ_{13})	-0.249589606	1.195026145	-0.014939656	0.050975224	…	0.983725805
f(realcompθ_{14})	-0.887365276	1.537972707	0.006088572	0.320426115	…	1.456473095
f(realcompθ_{15})	-1.417043617	1.161330687	0.021007591	0.060317371	…	1.249301843
f(realcompθ_{16})	-1.775551063	0.244695195	0.014992871	-0.298954699	…	0.431113749

Table 24 shows the results of the complex multiply realized for each point for the imaginary part. For example, for point 1 of f(realcompθ_1), which is the complex multiply for the real part of θ_1, the following was performed:

$$f(imagcomp\theta_{1,1}) = (-I_{1,\theta1} \times I_{1d}) + (R_{1,\theta1} \times Q_{1d})$$

$$f(imagcomp\theta_{1,1}) = [(-f(imag\theta_{1,1})) \times f(I\theta_{1,1})] + [f(real\theta_{1,1}) \times f(Q\theta_{1,1})]$$

$$f(imagcomp\theta_{1,1}) = [(-(-0.495353314))(1.908679)] + [(-0.868691599)(-0.2372)]$$
$$= 1.151524027$$

Table 24. Imaginary Part after Complex Multiply

	1	2	3	4	…	16
f(imagcompθ_1)	1.151524027	0.516472965	0.015091307	-0.190330301	…	-0.570344702
f(imagcompθ_2)	1.607790776	1.32522935	0.020974707	-0.287583943	…	-1.321219366
f(imagcompθ_3)	1.871721668	1.517335268	0.00595697	0.088872233	…	-1.427571111
f(imagcompθ_4)	1.910178909	0.999222582	-0.015038416	0.318595027	…	-0.868719878
f(imagcompθ_5)	1.717336902	0.011034844	-0.020960976	0.020249076	…	0.077896671
f(imagcompθ_6)	1.315731991	-0.983347749	-0.005800519	-0.311828475	…	0.982014298
f(imagcompθ_7)	0.753719402	-1.514479959	0.015213736	-0.124989192	…	1.451411062
f(imagcompθ_8)	0.099617378	-1.330426334	0.020884125	0.27012754	…	1.290928892
f(imagcompθ_9)	-0.566733845	-0.517547578	0.005472295	0.214939106	…	0.574375733
f(imagcompθ_{10})	-1.163917126	0.539787265	-0.015461715	-0.198550783	…	-0.390866071
f(imagcompθ_{11})	-1.619098804	1.341789187	-0.020793424	-0.281209319	…	-1.189876916
f(imagcompθ_{12})	-1.877084243	1.510581554	-0.005177186	0.104077566	…	-1.470487059
f(imagcompθ_{13})	-1.907098243	0.968511461	0.015632229	0.316374846	…	-1.095235954
f(imagcompθ_{14})	-1.706429473	-0.027237687	0.020748233	0.004315226	…	-0.214346396
f(imagcompθ_{15})	-1.300502236	-1.008668912	0.0051226	-0.314727392	…	0.778783128
f(imagcompθ_{16})	-0.739416732	-1.518626419	-0.015581197	-0.115401926	…	1.407621821

The sum column of Table 25 shows the sum of all the points for each of the functions for the real part after the complex multiply, while the amplitude column shows the squared value of the sum column and corresponds to the amplitude at that angle for the real part.

Table 25. Amplitude for the Real Part of the Sixteen Functions

	Sum	Amplitude
f(reθ_1)	-3.33835	11.14456
f(reθ_2)	-3.88689	15.10794
f(reθ_3)	-4.55195	20.72023
f(reθ_4)	12.7253	161.9332
f(reθ_5)	-5.87817	34.55291
f(reθ_6)	11.53089	132.9615
f(reθ_7)	-6.74129	45.44499
f(reθ_8)	11.01314	121.2893
f(reθ_9)	-6.83565	46.72605
f(reθ_{10})	-6.57585	43.2418
f(reθ_{11})	11.78912	138.9833
f(reθ_{12})	-5.5526	30.83138
f(reθ_{13})	-4.8835	23.84862
f(reθ_{14})	13.80013	190.4435

f(reθ_{15})	-3.58281	12.83653
f(reθ_{16})	-3.12353	9.756424

The sum column of Table 26 shows the sum of all the points for each of the functions for the imaginary part after the complex multiply, while the amplitude column shows the squared value of the sum column and corresponds to the amplitude at that angle for the imaginary part.

Table 26. Amplitude for the Imaginary Part of the Sixteen Functions

	Sum	**Amplitude**
f(imθ_1)	1.205185	1.452472
f(imθ_2)	1.689652	2.854924
f(imθ_3)	1.941031	3.767601
f(imθ_4)	1.94733	3.792094
f(imθ_5)	1.726221	2.979838
f(imθ_6)	1.316284	1.732605
f(imθ_7)	0.769561	0.592223
f(imθ_8)	0.145789	0.021254
f(imθ_9)	-0.49186	0.241926
f(imθ_{10})	-1.08008	1.16658
f(imθ_{11})	-1.55844	2.428739
f(imθ_{12})	-1.87273	3.507111
f(imθ_{13})	-1.97933	3.917742
f(imθ_{14})	-1.85096	3.42606
f(imθ_{15})	-1.48384	2.201794
f(imθ_{16})	-0.90565	0.820196

The following Table 27 shows each amplitude that correspond to each of the corresponding sixteen angles by using Equation 20 in which $real_{\theta n}$ represents the amplitude for the real part and $imag_{\theta n}$ represents the amplitude for the imaginary part.

$$A_n = 20 \times \log\left[(real_{\theta n} + imag_{\theta n})^{1/2}\right]$$

Equation 20: Amplitude Calculation for Each Angle

Table 27. Corresponding Amplitudes for each Angle

Amplitude	**Theta**
11.00268101	-8
12.54375538	-6.9333
13.88950329	-5.8667
22.19388739	-4.8
15.74410412	-3.7333

21.29348537	-2.6667
16.63108983	-1.6
20.83898545	-0.5333
16.71801857	0.53333
16.47464885	1.6
21.50486346	2.66667
15.3578126	3.73333
14.4351896	4.8
22.87509704	5.86667
11.7719943	6.93333
10.24346885	8

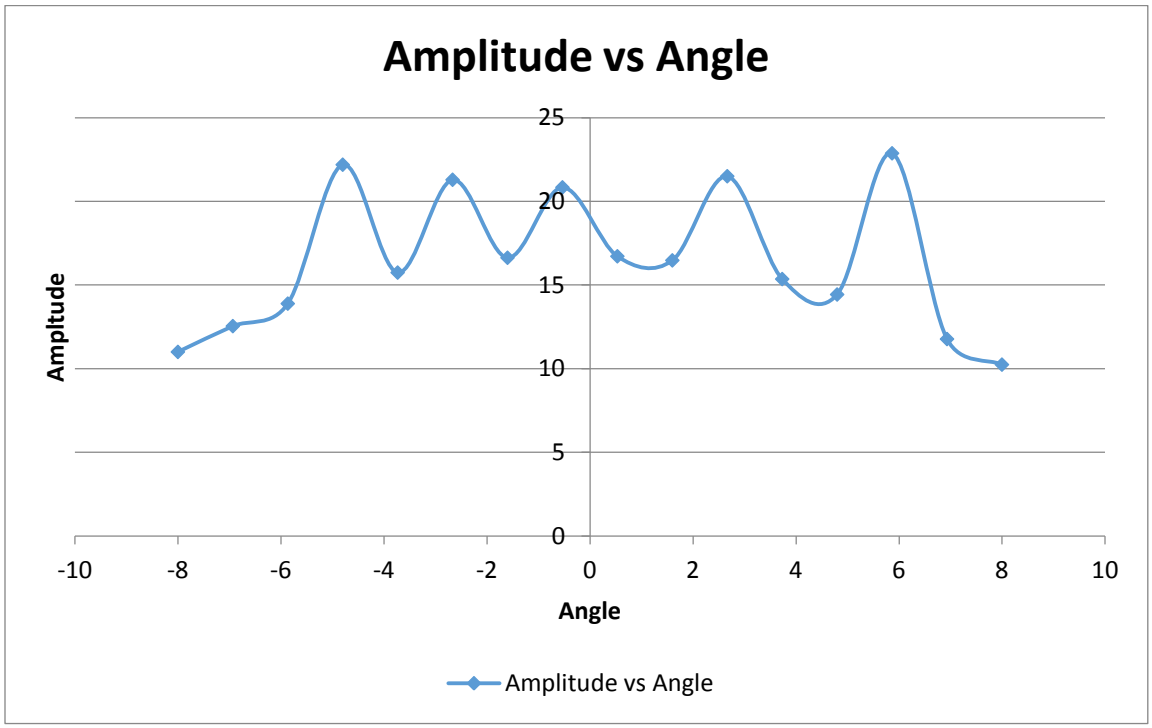

Figure 29. Amplitude vs Angle Graph

Figure 29 shows the graph for the amplitude vs angle that were obtained from all the calculations realized. It is basically the 1-dimensional image, which tells the used where the energy is coming in from different angles in the scene. Since there was energy coming in at five different angles for this example, each of the five peaks of the figure represents that information. When forming the image out of the five peaks, the display would have five strikes across it, informing the user that there is energy coming in from those five angles.

A2 House of Quality

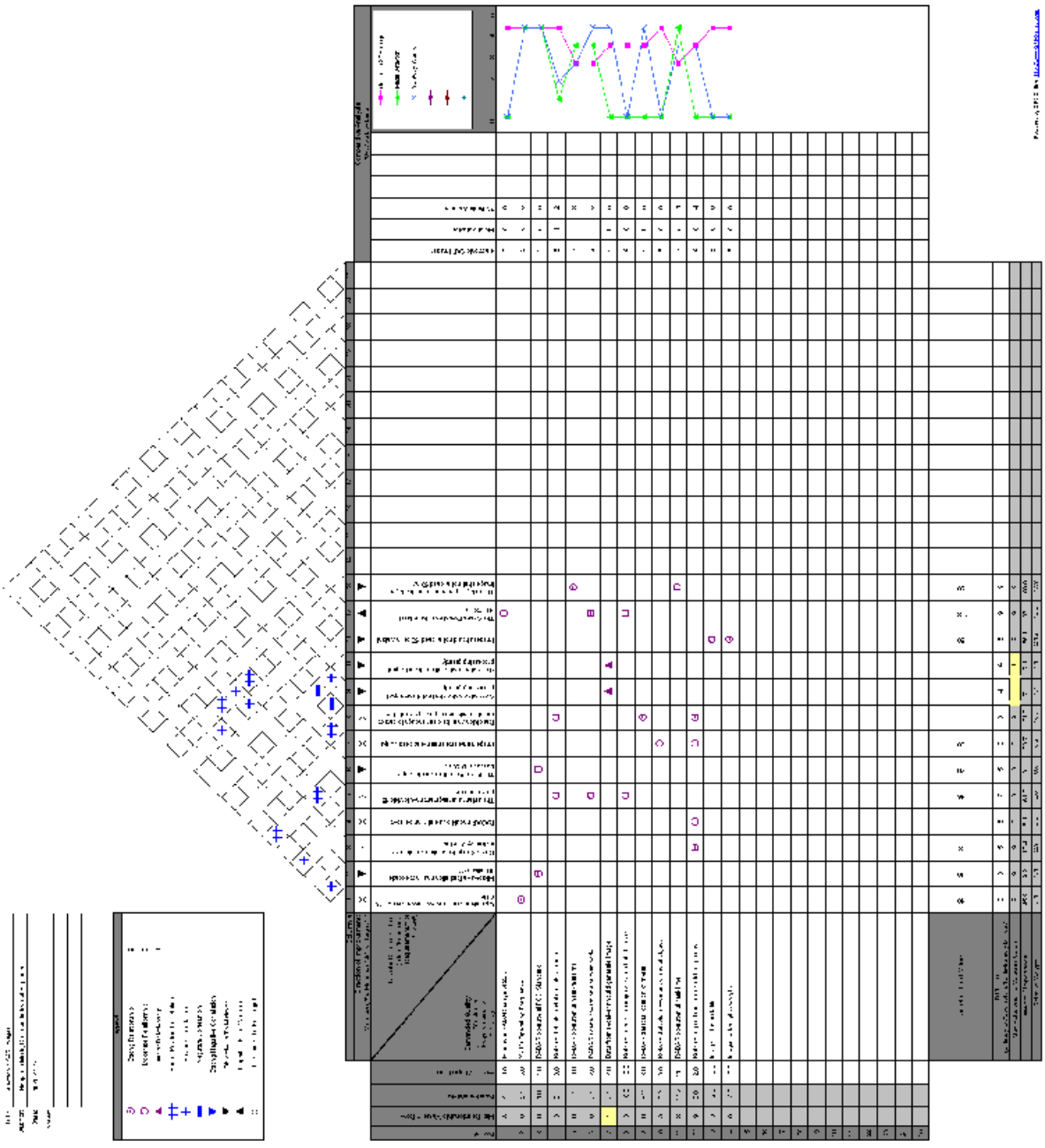

A3 Gantt Chart

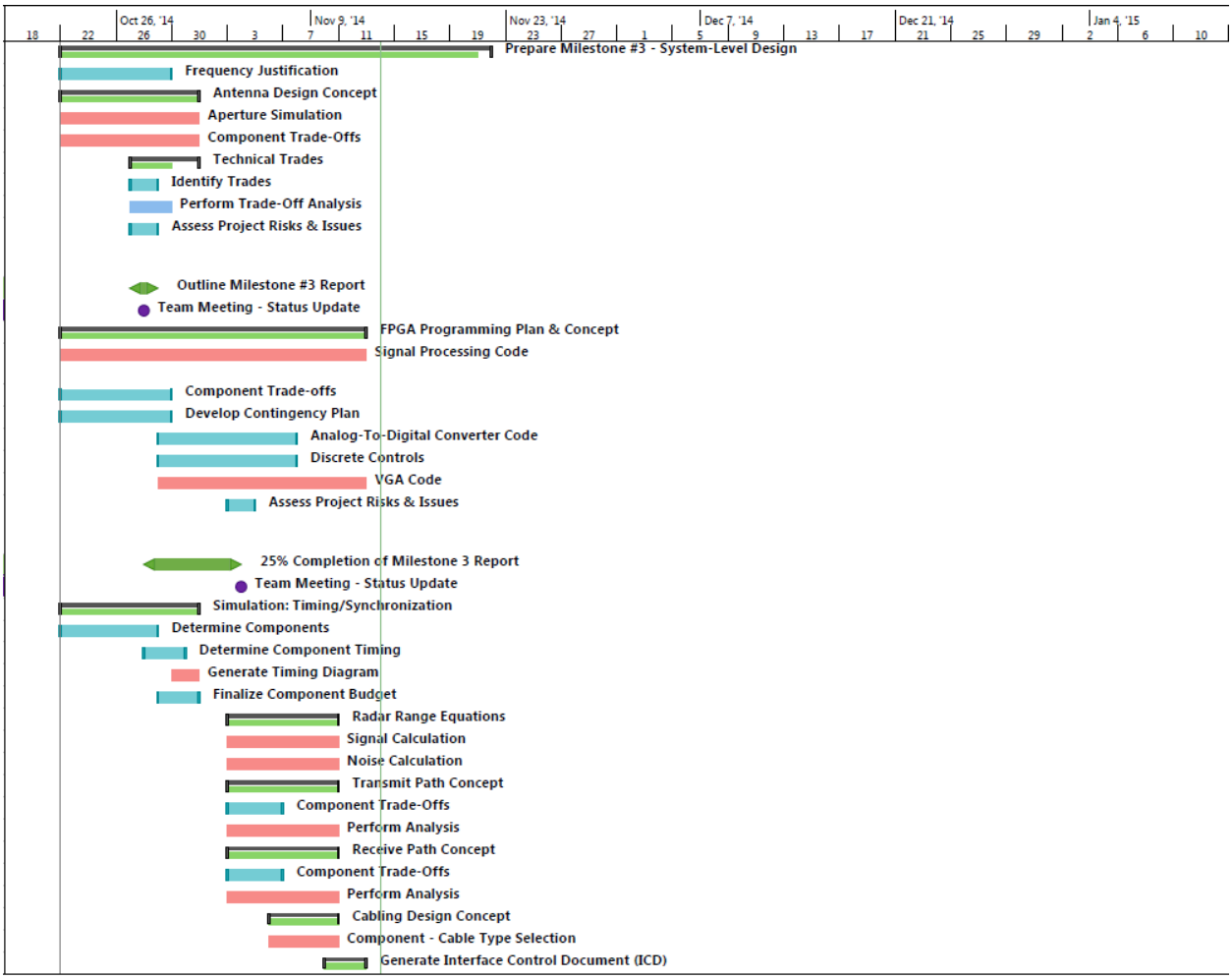

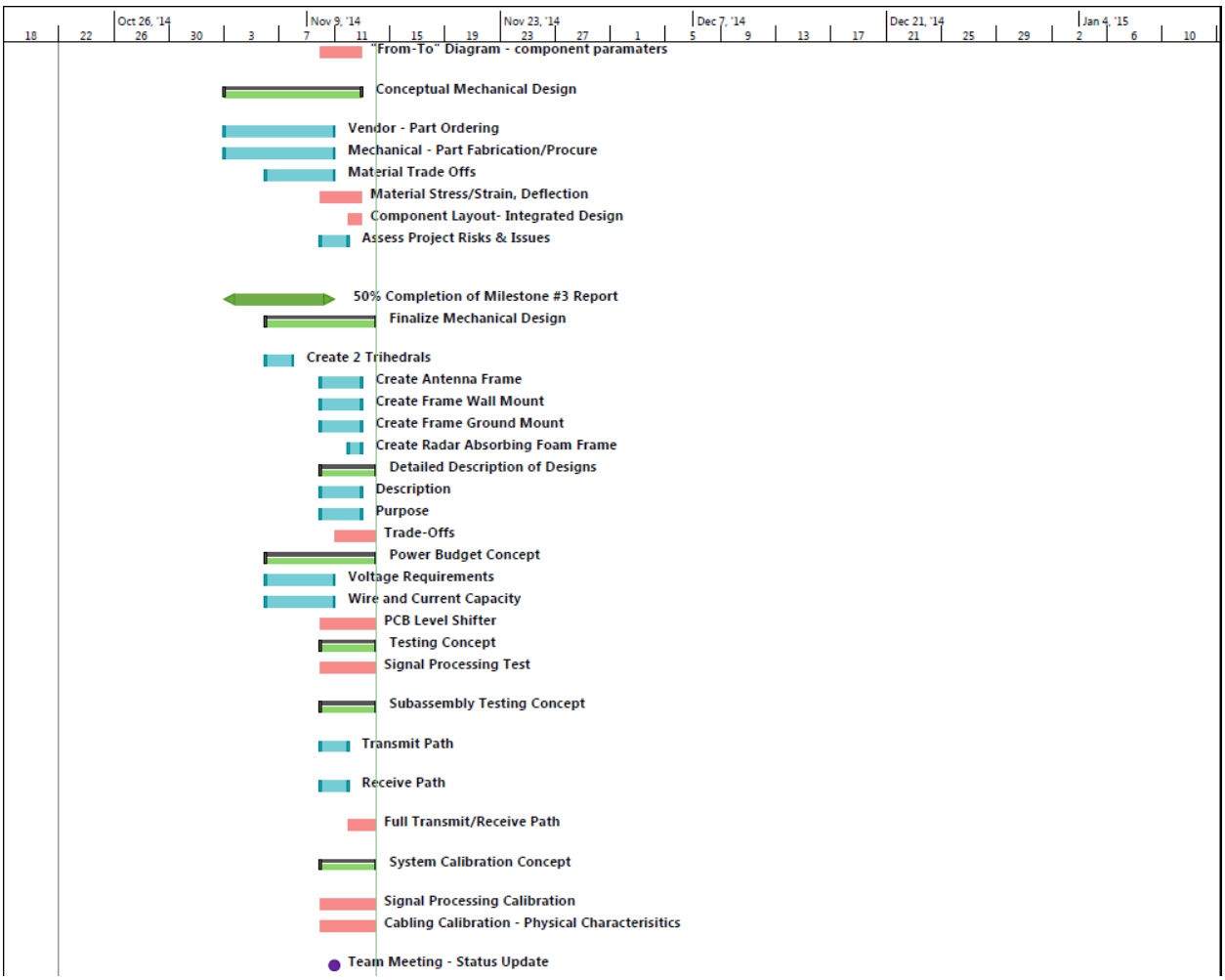
Oct 26, '14
Nov 9, '14
Nov 23, '14
Dec 7, '14
Dec 21, '14
Jan 4, '15
18 22 26 30 3 7 11 15 19 23 27 1 5 9 13 17 21 25 29 2 6 10
"From-To" Diagram - component paramaters
Conceptual Mechanical Design
Vendor - Part Ordering
Mechanical - Part Fabrication/Procure
Material Trade Offs
Material Stress/Strain, Deflection
Component Layout- Integrated Design
Assess Project Risks & Issues
50% Completion of Milestone #3 Report
Finalize Mechanical Design
Create 2 Trihedrals
Create Antenna Frame
Create Frame Wall Mount
Create Frame Ground Mount
Create Radar Absorbing Foam Frame
Detailed Description of Designs
Description
Purpose
Trade-Offs
Power Budget Concept
Voltage Requirements
Wire and Current Capacity
PCB Level Shifter
Testing Concept
Signal Processing Test
Subassembly Testing Concept
Transmit Path
Receive Path
Full Transmit/Receive Path
System Calibration Concept
Signal Processing Calibration
Cabling Calibration - Physical Characterisitics
Team Meeting - Status Update

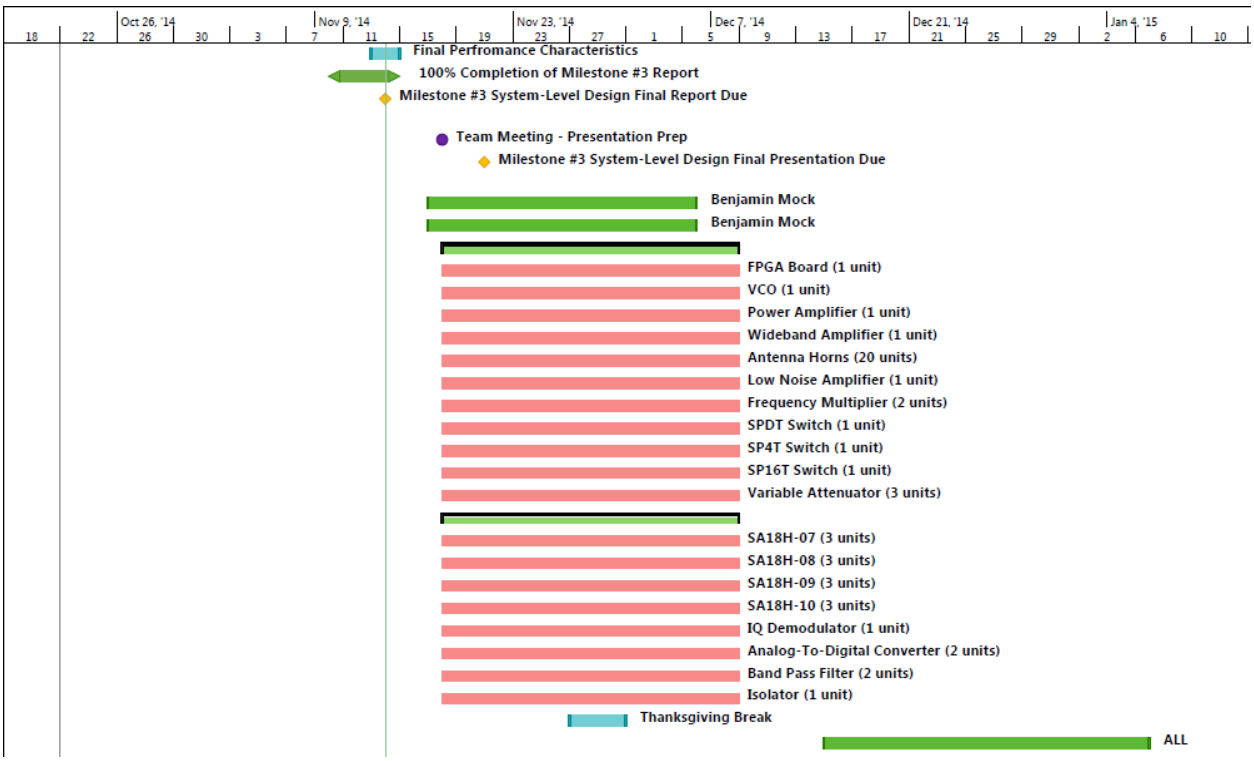
Oct 26, '14
Nov 9, '14
Nov 23, '14
Dec 7, '14
Dec 21, '14
Jan 4, '15
18 22 26 30 3 7 11 15 19 23 27 1 5 9 13 17 21 25 29 2 6 10
Final Perfromance Characteristics
100% Completion of Milestone #3 Report
Milestone #3 System-Level Design Final Report Due
Team Meeting - Presentation Prep
Milestone #3 System-Level Design Final Presentation Due
Benjamin Mock
Benjamin Mock
FPGA Board (1 unit)
VCO (1 unit)
Power Amplifier (1 unit)
Wideband Amplifier (1 unit)
Antenna Horns (20 units)
Low Noise Amplifier (1 unit)
Frequency Multiplier (2 units)
SPDT Switch (1 unit)
SP4T Switch (1 unit)
SP16T Switch (1 unit)
Variable Attenuator (3 units)
SA18H-07 (3 units)
SA18H-08 (3 units)
SA18H-09 (3 units)
SA18H-10 (3 units)
IQ Demodulator (1 unit)
Analog-To-Digital Converter (2 units)
Band Pass Filter (2 units)
Isolator (1 unit)
Thanksgiving Break
ALL

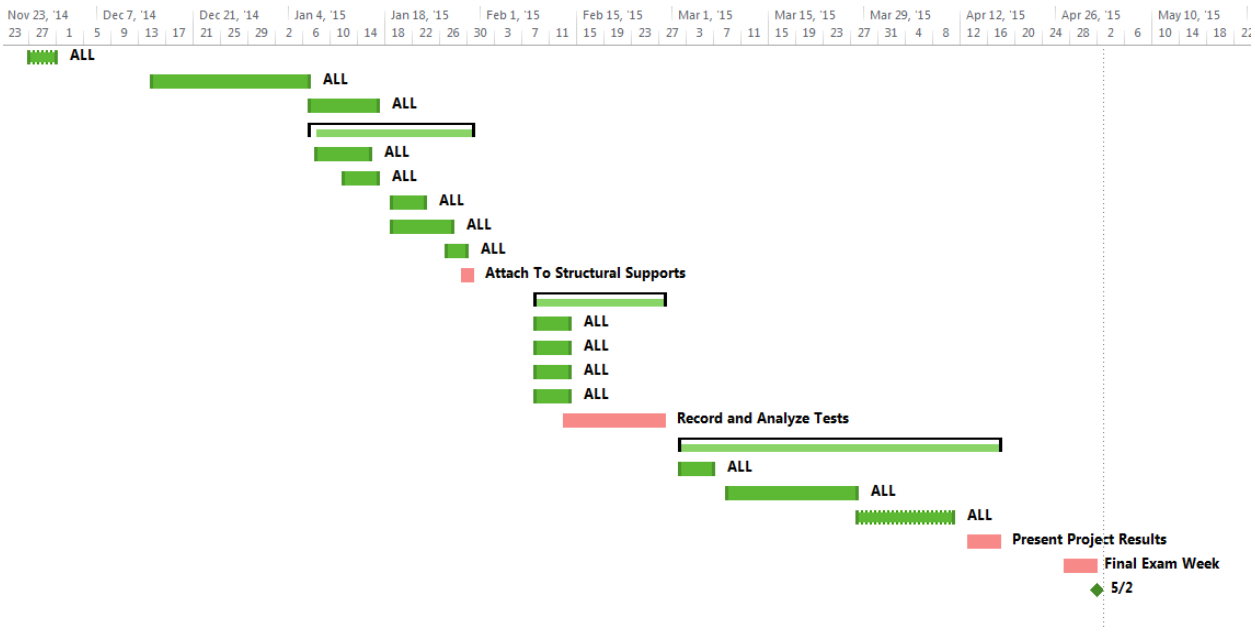
Nov 23, '14
Dec 7, '14
Dec 21, '14
Jan 4, '15
Jan 18, '15
Feb 1, '15
Feb 15, '15
Mar 1, '15
Mar 15, '15
Mar 29, '15
Apr 12, '15
Apr 26, '15
May 10, '15
ALL
ALL
ALL
ALL
ALL
ALL
ALL
ALL
Attach To Structural Supports
ALL
ALL
ALL
ALL
Record and Analyze Tests
ALL
ALL
ALL
Present Project Results
Final Exam Week
5/2